Time-Invariant Joint Transmit and Receive Beampattern Optimization for Polarization-Subarray Based Frequency Diverse Array Radar

Shiqi Gong, *Student Member, IEEE*, Shuai Wang, *Member, IEEE*, Sheng Chen, *Fellow, IEEE*, Chengwen Xing, *Member, IEEE*, and Xing Wei

***Abstract*—We propose a polarization-subarray based frequency diverse array (FDA) radar with the subarray-based FDA as the transmit (Tx) array and the polarization-sensitive subarray-based FDA (PSFDA) as the receive (Rx) array. The subarray-based FDA has the capability to achieve a single maximum beampattern at the target location, while the PSFDA can provide an extra degree of freedom to further suppress the interference and, thus, to improve the radar's signal-to-interference-plus-noise ratio (SINR). The time-dependent frequency offsets are designed for the proposed radar to realize the time-invariant beampattern at the desired target location over the whole pulse duration. To further improve the target detection performance, the time-invariant joint Tx–Rx beampattern design is considered based on the output SINR maximization. To effectively solve the nonconvex output SINR maximization problem, a suboptimal alternating optimization algorithm is proposed to iteratively optimize the FDA Tx beamforming, the PSFDA spatial pointings, and the PSFDA Rx beamforming. Numerical experiments illustrate that the time-invariant and single-maximum joint Tx–Rx beampattern at the target location is achieved. Moreover, compared to the basic FDA and logarithmic frequency offset FDA as well as conventional phased array radars, the proposed polarization-subarray based FDA radar achieves a significant SINR improvement, particularly when the desired target and the interferences are spatially indistinguishable.**

***Index Terms*—Polarization-subarray based FDA radar, joint transmit-receive beampattern design, time-invariant beampattern, output SINR maximization.**

I. Introduction

TRADITIONALLY, phased-array (PA) has been widely accepted as an efficient way to detect targets in various communication and radar systems, because it has the capability to electronically steer a high gain beam to the desired direction. However, PA is not sensitive to the range, and can only provide the time-modulated beam at a specific angle for all ranges. Recently, much attentions have been focused on the range-dependent beampattern design in many applications, such as the range-dependent interference and ambiguity suppression, and the range-dependent target tracking [1]. To achieve this goal, a flexible array, referred to as frequency diverse array (FDA), was proposed in [2], [3]. Different from PA and multiple-input multiple-output (MIMO) array [4] which have the same carrier frequency for every antenna element, the FDA achieves the range-angle-time dependent beampattern by introducing the frequency offset across all array elements. Generally, the frequency offset of each array element is much smaller than the carrier frequency. Moreover, the FDA is different from the frequency scanning array, whose carrier frequency is time-modulated [5], and it is also different from the conventional frequency hopping strategy [6].

The FDA beampattern periodicity, in terms of angle, range and time, was proved in [7], [8], and many potential applications of FDA were reported in [9]–[13]. Specifically, the work in [9] demonstrated that the FDA can be utilized to detect the relatively low velocity moving objectives, and the FDA multipath characteristics over a ground plane were explored in [10], which also indicates that the FDA can perform multiple missions simultaneously by exploiting the degrees-of-freedom of time, frequency and space region. To show the advantage of FDA in target detection, a range-angle dependent beampattern synthesis method was proposed in [11] to focus the FDA transmit (Tx) energy on the desired target direction and to effectively suppress the range-dependent interference. It was note that the FDA can also be combined with the MIMO radar for deceptive jamming and clutter suppression [12], [13]. For example, in [13], the adaptive range-angle-Doppler processing approach was proposed to address the range ambiguity issue.

However, the range-angle coupled beampattern characteristics of FDA are generally undesired in applications, and many published works have studied the decoupled range-angle FDA beampattern design in order to uniquely determine the target location. Up to date, two techniques are mainly considered to decouple the range-angle FDA beampattern [14]–[18]. The first approach is based on nonlinear frequency offset design [14], [15]. For example, in [14], the nonlinear logarithmic frequency offset (LFO) was proposed to achieve the unique target localization, while in [15], a novel random frequency diverse array was

Manuscript received March 19, 2018; revised July 5, 2018; accepted August 21, 2018. Date of publication September 6, 2018; date of current version September 14, 2018. The associate editor coordinating the review of this manuscript and approving it for publication was Dr. Gang Li. This work was supported in part by the National Natural Science Foundation of China under Grants 61620106001, 61671058, 61722104, and 61601524; in part by the Joint Foundation of National Natural Science Foundation of China and the General Purpose Technology Research Program under contract U1636125. *(Corresponding author: Shuai Wang.)*

S. Gong, S. Wang, C. Xing, and X. Wei are with the School of Information and Electronics, Beijing Institute of Technology, Beijing 100081, China (e-mail: gsqyx@163.com; swang@bit.edu.cn; chengwenxing@ieee.org; weixing_2015@foxmail.com).

S. Chen is with the School of Electronics and Computer Science, University of Southampton, Southampton SO17 1BJ, U.K., and also with King Abdulaziz University, Jeddah 21589, Saudi Arabia (e-mail: sqc@ecs.soton.ac.uk).

Color versions of one or more of the figures in this paper are available online at http://ieeexplore.ieee.org.

Digital Object Identifier 10.1109/TSP.2018.2868041

designed by randomly assigning the carrier frequency for each array element in order to derive an uncoupled and stochastic range-angle beampattern. The other approach exploits the specific structure of FDA. Specifically, in [16], [17], the subarray-based FDA with different frequency offsets was proposed to realize the single-maximum beampattern at the target location, and the corresponding target detection performance were analyzed via the minimum mean square error (MMSE) and Cramér-Rao lower bound (CRLB) metrics. By combining the both approaches, a novel subarray-based MIMO-FDA radar with LFO was proposed in [18] for multiple-target localization in different range bins.

It is clear that the aforementioned FDA literature [12]–[14], [16]–[18] can tackle the range and angle dependent interference effectively. Nevertheless, the FDA actually produces the time-modulated range-angle dependent beampattern. Although the signal-to-interference-plus-noise ratio (SINR) loss due to the range-angle periodicity can be mitigated [14], [16]–[18], the SINR loss caused by the periodicity in time is still not addressed in most of the FDA related works. For example, in [7], the time-dependent FDA beampattern characteristics are simulated, but it does not tackle the time-variant issues. To tackle this issue, the work in [19] firstly designed a time-dependent frequency offset to achieve the time-independent FDA transmit beampattern. A more general time-modulated frequency offset scheme was proposed in [20] to realize the time-invariant FDA spatial focusing beampattern. Besides, the influence of frequency offset errors on the FDA time-invariant beampattern design was also studied in [20].

In fact, all the above mentioned arrays are actually scalar arrays, which can only extract the signal amplitude and phase information for further processing. However, it is known that the signal polarization information is also a nature property of electromagnetic (EM) waves [21]. Existing works [22]–[25] have indicated that the target localization performance can be improved by utilizing the polarization difference among signals. In general, polarization is an important property not only for radio frequency (RF) signals but also for RF antennas. Specifically, for most RF antennas, the polarization is defined by the corresponding antenna pointings. For example, an antenna with horizontal/vertical pointing receives horizontally/vertically polarized signals best [22], [23]. Therefore, it is important to match the polarization of RF antennas to that of the incoming signal for the best reception. Most of the existing works [22]–[25] studied a special vector array, called polarization sensitive array (PSA), which is capable of exploiting the signal polarization information. Different from the conventional PA and the basic FDA, PSA is composed of a number of antennas with different spatial pointings, which represent the array polarization sensitivity and can effectively receive signals with different polarizations in a vector way [25]. There exist very few literature considering the combination of PSA and FDA, which we refer to as the PSFDA. An exception is the work [26], in which the sparse reconstruction based angle-range-polarization beamforming was designed for the PSFDA to provide good range-polarization resolution.

Against the above background, in this paper, we propose a polarization-subarray based FDA radar for detecting the target in the existence of multiple interferences. Specifically, we adopt the subarray-based FDA and the subarray-based PSFDA as the Tx array and the receive (Rx) array, respectively. The joint Tx-Rx beampattern is then designed for the proposed polarization-subarray based FDA radar. Traditionally, the joint Tx-Rx beampattern design for radar systems only considers the optimization of the Tx and Rx beamforming based on the direction of arrivals (DOAs) information of the target signal and the interferences [27]–[29]. However, when the target signal and the interferences are spatially indistinguishable, this type of beampattern design will not work. This is because the achievable output SINR by this joint Tx-Rx beampattern design is very low owing to the similar steering vectors of the target signal and the interferences. In this context, the polarization difference among the target signal and the interferences can be utilized to enhance the output SINR. Therefore, in our work, the polarization of the subarray-based PSFDA, namely, the Rx PSFDA spatial pointings, is also optimized to sufficiently match with that of the target signal, while maintaining orthogonal to the polarization of the interferences as much as possible. Specifically, based on the time-dependent frequency offsets design, we iteratively optimize the FDA Tx beamforming, the PSFDA spatial pointings and the PSFDA Rx beamforming to realize the single-maximum and time-invariant joint Tx-Rx beampattern at target location. Our main contributions are summarized as follows:

- To the authors' best knowledge, this paper is the first to propose the polarization-subarray based FDA radar. In this radar system, the subarray-based Tx FDA is capable of achieving the single-maximum and range-angle decoupled beampattern at the target. By further introducing the polarization sensitivity to the subarray-based Rx FDA, the interferences can be effectively suppressed even when they are spatially very close to the desired target signal impinging on the Rx array. Consequently, the proposed polarization-subarray based FDA radar significantly improves the target detection performance.
- Since a time-varying beampattern is generally undesired in target detection, we design the time-dependent frequency offset for the polarization-subarray based FDA radar by extending the design of [20] for the basic FDA radar, which is capable of realizing the time-invariant spatially focusing beampattern at the desired target location during the whole pulse duration.
- To further improve the target detection performance, the optimal joint Tx-Rx beampattern of the polarization-subarray based FDA radar is investigated based on the output SINR maximization. Since this maximization problem is nonconvex and generally intractable, we propose an efficient alternating optimization algorithm to iteratively optimize the FDA Tx beamforming, the PSFDA spatial pointings and the PSFDA Rx beamforming. It is worth emphasizing again that because the PSFDA spatial pointings are optimized, the polarization-subarray based FDA can effectively utilize the polarization difference among the signals to enhance the target detection performance, particularly when the desired target signal and the interfering signals are spatially indistinguishable.

Although the work in [26] also considers the PSFDA, it is evidently different from our work in three aspects. Firstly, in [26], only the MVDR Tx beamforming is designed based on the sparse constraints, while the Rx beamforming optimization is not considered for sidelobes suppression. Secondly, the polarization of the PSFDA in [26] is determined by the dual-polarized array, which is generally not optimal for distinguishing the target and the interferences in the polarization domain. Thirdly, the issue of the range-angle coupled beampattern for the basic FDA

is not addressed in [26], and thus it may cause the ambiguity in target detection.

Throughout our discussions, normal-faced lower-case letters denote scalars, while bold-faced lower-case and upper-case letters denote vectors and matrices, respectively. Absolute value and Euclidean norm are denoted by $|\cdot|$ and $\|\cdot\|$, respectively, while $(\cdot)^*$, $(\cdot)^{\mathrm{T}}$, $(\cdot)^{\mathrm{H}}$ and $(\cdot)^{-1}$ represent the conjugate, transpose, conjugate transpose and inverse operators, respectively. $\mathrm{Tr}(\cdot)$ and $\mathrm{rank}(\cdot)$ denote the trace and rank of matrix, respectively, while $\mathrm{j} = \sqrt{-1}$. The Hadmard and Kronecker product operators are denoted by $\odot$ and $\otimes$, respectively, while $\mathrm{diag}(\boldsymbol{b}) \in \mathbb{C}^{N\times N}$ is the diagonal matrix whose diagonal elements are the elements of $\boldsymbol{b} \in \mathbb{C}^N$. $\boldsymbol{I}_N$ is the $N \times N$ identity matrix, and $\mathbf{1}_N$ is the N-dimensional vector whose elements are all equal to 1, while $\mathbf{0}_{n\times m}$ is the $n \times m$ zero matrix. $\boldsymbol{A} \succeq 0$ indicates that $\boldsymbol{A}$ is a positive semidefinite matrix, and $\mathsf{E}[\cdot]$ is the expectation operator, while $\boldsymbol{a}|_{[m:n]}$ denotes the m-th element to the n-th element of the vector $\boldsymbol{a}$. The phrase 'with respect to' is abbreviated as 'w.r.t.'.

II. Radar Model and Problem Formulation

A. Proposed Polarization-Subarray Based FDA Radar

We consider a monostatic narrowband FDA radar system. It is known that the basic FDA has a coupled range-angle beampattern, which makes the independent range and angle estimation of a far field target impossible. The subarray-based FDA can be employed to decouple the range-angle dependent beampattern by properly choosing the frequency offset of each FDA subarray [16]. Besides, partitioning a large-scale antenna array into identical-size subarrays with mass production can significantly reduce the hardware cost [16], [17]. Therefore, in our proposed FDA radar system, the Tx array consists of two equal-size FDA subarrays, each FDA subarray having N array elements, while the Rx array consists of two equal-size polarization-sensitive FDA subarrays, each subarray having N array elements too.[1] This proposed FDA radar is called the polarization-subarray based FDA radar. For simplicity, both the Tx and Rx arrays' antenna spacings are set to be d.

It is assumed that there exist one desired target and K interference sources located at (θ_0, R_0) and (θ_k, R_k), $1 \le k \le K$, respectively, in the far field, as illustrated in Fig. 1. Since this is a monostatic radar system, the locations of each source signal w.r.t. the both Tx and Rx arrays are the same. Additionally, we also assume that the target and the interference sources are located in the same/nearby range cell, whose range width is defined as $r_p = \frac{c_0}{2B}$ with c_0 and B denoting the light speed and the waveform bandwidth, respectively. In order to detect the target effectively, the corresponding interference sidelobes should be sufficiently suppressed. If these interference positions are unknown, they can be detected prior to the target sensing as suggested in [28]. The carrier frequency for all the subarrays in this radar is f_0, while the frequency offsets of the first Tx/Rx subarray and the second Tx/Rx subarray are set to Δf_1 and Δf_2,

[1]Our work aims to utilize different frequency offsets of FDA subarrays to realize the range-angle decoupled beampattern, which is actually not related to the size of subarrays. Also to achieve the range-angle decoupled beampattern, it is sufficient to use two FDA subarrays. Our work can readily be extended to the case of unequal-size subarrays at both the Tx and Rx arrays by slightly modifying the PSFDA received signal model (17), and all the results of this paper are still applicable.

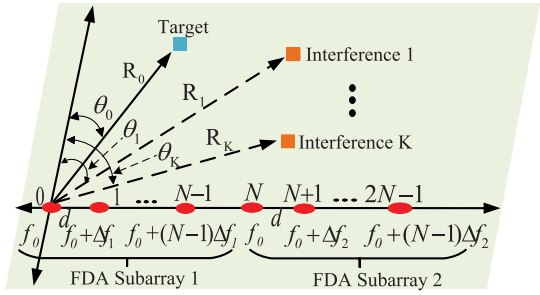

Fig. 1. Illustration of the two-subarray-based FDA radar transmitter, where there exist one desired target and K interference sources.

respectively, which satisfy

$$|(N-1)\Delta f_1| \ll f_0,\ |(N-1)\Delta f_2| \ll f_0. \tag{1}$$

Therefore, the $(n+1)$-th antenna carrier frequency f_n of the subarray-based Tx FDA is expressed as

$$f_n = \begin{cases} f_0 + n\Delta f_1, & n \in \{0, 1, \ldots, N-1\}, \\ f_0 + (n-N)\Delta f_2, & n \in \{N, N+1, \ldots, 2N-1\}. \end{cases} \tag{2}$$

The baseband equivalent model of the transmitted signal vector $\widetilde{\boldsymbol{s}}_{Tx}(t) \in \mathbb{C}^{2N}$ from the $2N$ Tx FDA antennas is given by

$$\widetilde{\boldsymbol{s}}_{Tx}(t) = \boldsymbol{w}_{Tx} s_{Tx}(t),\ t \in [0,\ T_p], \tag{3}$$

where $s_{Tx}(t)$ is the transmitted pulse waveform with the pulse duration T_p, and $\boldsymbol{w}_{Tx} = \left[w_{Tx}^0\ w_{Tx}^1 \cdots w_{Tx}^{(2N-1)}\right]^{\mathrm{T}} \in \mathbb{C}^{2N}$ with $\|\boldsymbol{w}_{Tx}\|^2 = 1$ is the unit-norm Tx beamforming vector of the subarray-based FDA.

Let the first antenna of the subarray-based Tx FDA be the reference antenna. Then the received signal at the spatial location (θ, R) from the subarray-based Tx FDA can be formulated as a linear combination of the $2N$ attenuated and delayed versions of the Tx signal $s_{Tx}(t)$, where (θ, R) are the DOA and the range of this location relative to the reference antenna of the subarray-based Tx FDA. Furthermore, based on the narrowband assumption, the baseband equivalence of the received signal at location (θ, R) can be expressed as

$$\begin{aligned} s_{Rx}(t;\theta,R) &\approx \boldsymbol{a}^{\mathrm{T}}(t;\theta,R)\widetilde{\boldsymbol{s}}_{Tx}\left(t - \frac{R}{c_0}\right) \\ &= \boldsymbol{a}^{\mathrm{T}}(t;\theta,R)\boldsymbol{w}_{Tx} s_{Tx}\left(t - \frac{R}{c_0}\right), \end{aligned} \tag{4}$$

where $\boldsymbol{a}(t;\theta,R) \in \mathbb{C}^{2N}$ is the steering vector of the Tx subarray-based FDA, which consists of $2N$ propagation phase shifts. More specifically,

$$\boldsymbol{a}(t;\theta,R) = \left[1\, e^{\mathrm{j}\varphi_1(t)} \cdots e^{\mathrm{j}\varphi_{2N-1}(t)}\right]^{\mathrm{T}}, \tag{5}$$

with

$$\varphi_n(t) = \begin{cases} 2\pi n k_0 d \sin\theta + 2\pi n \Delta f_1 (t - \tau_n), \\ \quad n \in \{0, 1, \ldots, N-1\}, \\ 2\pi n k_0 d \sin\theta + 2\pi (n-N) \Delta f_2 (t - \tau_n), \\ \quad n \in \{N, N+1, \ldots, 2N-1\}, \end{cases} \tag{6}$$

where $k_0 = \frac{f_0}{c_0}$ and $\tau_n = \frac{R - n d \sin\theta}{c_0}$.

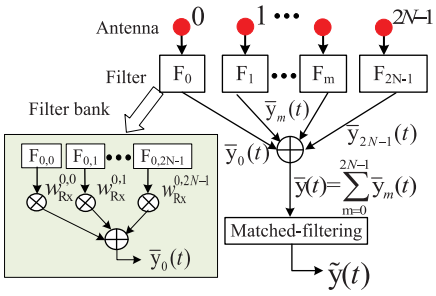

Fig. 2. Polarization-sensitive two-subarray based FDA radar receiver.

The polarization-sensitive two-subarray based FDA radar receiver is shown in Fig. 2, where each PSFDA antenna receives all the Tx signals from the subarray-based Tx FDA through a filter bank. Specifically, the filter bank of the $(m+1)$-th PSFDA antenna, $0 \le m \le 2N-1$, consists of the transfer functions $\mathrm{F_{m,n}}$, $0 \le n \le 2N-1$, which effectively receives the signal with the radiation frequency f_n from the $(n+1)$-th antenna of the subarray-based Tx FDA and weights it with the weighting factor $w_{Rx}^{m,n}$. Consequently, the maximum received SINR at the Rx PSFDA can be achieved.

The signal impinges on a generic PSFDA from the DOA (θ, ϕ), where $\theta \in [0, \pi/2]$ and $\phi \in [0, 2\pi)$ are the elevation and azimuth angles, respectively. The corresponding transverse electric field of the impinging EM signal is expressed as

$$\boldsymbol{E}(t) = E_\theta(t)\boldsymbol{e}_\theta + E_\phi(t)\boldsymbol{e}_\phi, \tag{7}$$

where $E_\phi(t)$ and $E_\theta(t)$ are the electric field components in the directions of $\boldsymbol{e}_\phi$ and $\boldsymbol{e}_\theta$, respectively. Similar to [22], [25], we assume that a EM signal is completely polarized so that the time-varying $\boldsymbol{E}(t)$ can be modeled as a polarization ellipse with the polarization angle (POA) (α, β), in which α is the polarized rotation angle and β is the polarized ellipse angle. Then the signal polarization vector $\boldsymbol{e}(\boldsymbol{\delta})$ is defined by

$$\boldsymbol{e}(\boldsymbol{\delta}) = \boldsymbol{S}(\theta, \phi)\boldsymbol{R}(\alpha)\boldsymbol{g}(\beta), \tag{8}$$

where $\boldsymbol{\delta} = [\theta\, \phi\, \alpha\, \beta]^{\mathrm{T}}$ is the collection of the source signal's DOA and POA relative to the PSA, and $\boldsymbol{S}(\theta, \phi)$ is the steering matrix of the impinging polarized signal with DOA (θ, ϕ), which is expressed as

$$\boldsymbol{S}(\theta, \phi) = \begin{bmatrix} -\sin\phi & \cos\theta\cos\phi \\ \cos\phi & \cos\theta\sin\phi \\ 0 & -\sin\theta \end{bmatrix}, \tag{9}$$

while $\boldsymbol{R}(\alpha)$ is the polarized rotation matrix given by

$$\boldsymbol{R}(\alpha) = \begin{bmatrix} \cos\alpha & \sin\alpha \\ -\sin\alpha & \cos\alpha \end{bmatrix}, \tag{10}$$

and the polarized ellipse vector is

$$\boldsymbol{g}(\beta) = \begin{bmatrix} \cos\beta \\ \mathrm{j}\sin\beta \end{bmatrix}. \tag{11}$$

The polarization sensitive matrix $\boldsymbol{P}_e$ representing the array electric field gain for the impinging signal, also known as the array spatial pointings matrix, is defined as

$$\boldsymbol{P}_e = G_e \begin{bmatrix} \boldsymbol{p}_0 \\ \boldsymbol{p}_1 \\ \vdots \\ \boldsymbol{p}_{2N-1} \end{bmatrix} \in \mathbb{R}^{2N\times 3}, \tag{12}$$

where G_e denotes the array polarization gain when the polarization status of the impinging signal and the array perfectly match, $\boldsymbol{p}_n \in \mathbb{C}^{1\times 3}$ is the spatial pointing vector of the $(n+1)$-th antenna of the PSFDA with the antenna's elevation and azimuth angles $(\theta_{e,n}, \phi_{e,n})$, which is given by

$$\boldsymbol{p}_n = \left[\sin\phi_{e,n}\cos\theta_{e,n}\ \sin\phi_{e,n}\sin\theta_{e,n}\ \cos\phi_{e,n}\right], \tag{13}$$

for $0 \le n \le 2N-1$. It is naturally observed that the spatial pointing vector of each antenna satisfies $\|\boldsymbol{p}_n\| = 1$, for $0 \le n \le 2N-1$. Based on (8) and (12), the PSA's polarization vector $\boldsymbol{p}_e(\boldsymbol{\delta})$ is defined by

$$\boldsymbol{p}_e(\boldsymbol{\delta}) = \boldsymbol{P}_e\boldsymbol{e}(\boldsymbol{\delta}) \in \mathbb{C}^{2N}. \tag{14}$$

In this work, we mainly consider the uniform linear (UL) FDA radar having the one-dimensional DOA θ. This is equivalent to setting the azimuth angle $\phi = 90^\circ$ in $\boldsymbol{\delta}$. However, we also discuss the extension to the uniform rectangular planar (URP) FDA radar. Based on the receiver structure of Fig. 2, the steering vector of the subarray-based Rx PSFDA $\boldsymbol{b}(\theta, R) \in \mathbb{C}^{4N^2}$ can be expressed as

$$\boldsymbol{b}(\theta, R) = \left[e^{\mathrm{j}b_{0,0}} \cdots e^{\mathrm{j}b_{m,n}} \cdots e^{\mathrm{j}b_{(2N-1),(2N-1)}}\right]^{\mathrm{T}} \tag{15}$$

with $b_{m,n}$ for $m \in \{0, 1, \cdots 2N-1\}$ given by

$$b_{m,n} = \begin{cases} 2\pi m k_0 d\sin\theta - 2\pi n\Delta f_1\tau_m, \\ \quad n \in \{0, 1, \ldots, N-1\}, \\ 2\pi m k_0 d\sin\theta - 2\pi(n-N)\Delta f_2\tau_m, \\ \quad n \in \{N, N+1, \ldots, 2N-1\}. \end{cases} \tag{16}$$

$$\begin{aligned} \boldsymbol{y}(t) &= a_0\boldsymbol{B}(\theta_0, R_0)\Big(\boldsymbol{p}_e(\boldsymbol{\delta}_0) \otimes \big(\boldsymbol{a}(t;\theta_0, R_0) \odot \boldsymbol{w}_{Tx}\big)\Big)s_{Tx}\left(t - \frac{2R_0}{c_0}\right) \\ &\quad + \sum_{k=1}^{K} a_k\boldsymbol{B}(\theta_k, R_k)\Big(\boldsymbol{p}_e(\boldsymbol{\delta}_k) \otimes \big(\boldsymbol{a}(t;\theta_k, R_k) \odot \boldsymbol{w}_{Tx}\big)\Big)s_{Tx}\left(t - \frac{2R_k}{c_0}\right) + \boldsymbol{\xi}(t) \qquad (17a) \\ &= a_0\underbrace{\Big(\big(\widetilde{\boldsymbol{P}}_e(\boldsymbol{\delta}_0) \otimes \boldsymbol{A}(t;\theta_0, R_0)\big)\boldsymbol{b}(\theta_0, R_0)\Big)}_{\boldsymbol{a}_J(t;R_0,\boldsymbol{\delta}_0)} \odot \big(\mathbf{1}_{2N_r} \otimes \boldsymbol{w}_{Tx}\big)s_{Tx}\left(t - \frac{2R_0}{c_0}\right) \\ &\quad + \sum_{k=1}^{K} a_k\underbrace{\Big(\big(\widetilde{\boldsymbol{P}}_e(\boldsymbol{\delta}_k) \otimes \boldsymbol{A}(t;\theta_k, R_k)\big)\boldsymbol{b}(\theta_k, R_k)\Big)}_{\boldsymbol{a}_J(t;R_k,\boldsymbol{\delta}_k)} \odot \big(\mathbf{1}_{2N_r} \otimes \boldsymbol{w}_{Tx}\big)s_{Tx}\left(t - \frac{2R_k}{c_0}\right) + \boldsymbol{\xi}(t). \qquad (17b) \end{aligned}$$

In fact, $b_{m,n}$ represents the phase shift between the target signal with frequency f_n and the $(m+1)$-th Rx antenna of the PSFDA. By combining the received signal at location (θ, R) in (4), the PSA polarization vector in (14) and the steering vector of the subarray-based Rx PSFDA in (15), the baseband received signal $\boldsymbol{y}(t) \in \mathbb{C}^{4N^2}$ of the PSFDA can be expressed as (17) given at the bottom of the previous page. It is noted that the dimension of the received signal is $4N^2$ due to the full-band reception via the receiver structure of Fig. 2. In (17), a_0 and a_k, $\forall k$, are the complex amplitudes of the target and the k-th interference with the variances σ_0^2 and σ_k^2, respectively, while $\boldsymbol{\xi}(t) \in \mathbb{C}^{4N^2}$ is the additive Gaussian white noise (AWGN) vector with the covariance matrix $\sigma_\xi^2 \boldsymbol{I}_{4N^2}$. Generally, a_0 and a_k, $\forall k$, are mutually independent. Furthermore, in (17), we have $\boldsymbol{B}(\theta, R) = \mathrm{diag}(\boldsymbol{b}(\theta, R)) \in \mathbb{C}^{4N^2 \times 4N^2}$, and

$$\widetilde{\boldsymbol{P}}_e(\boldsymbol{\delta}) = \mathrm{diag}\big(\boldsymbol{p}_e(\boldsymbol{\delta})\big) \in \mathbb{C}^{2N \times 2N}, \tag{18}$$

$$\boldsymbol{A}(t; \theta, R) = \mathrm{diag}(\boldsymbol{a}(t; \theta, R)) \in \mathbb{C}^{2N \times 2N}. \tag{19}$$

In (17), we also define the joint Tx-Rx steering vector of the proposed polarization-subarray based FDA radar as

$$\boldsymbol{a}_J(t; R, \boldsymbol{\delta}) = \big(\widetilde{\boldsymbol{P}}_e(\boldsymbol{\delta}) \otimes \boldsymbol{A}(t; \theta, R)\big)\boldsymbol{b}(\theta, R) \in \mathbb{C}^{4N^2}. \tag{20}$$

As illustrated in Fig. 2, by performing the Rx beamforming with the unit-norm beamforming weighting vector $\boldsymbol{w}_{Rx} = \big[w_{Rx}^{0,0} \cdots w_{Rx}^{m,n} \cdots w_{Rx}^{(2N-1),(2N-1)}\big]^{\mathrm{T}} \in \mathbb{C}^{4N^2}$ on $\boldsymbol{y}(t)$, we further obtain the Rx beamforming output as $\bar{y}(t) = \boldsymbol{w}_{Rx}^{\mathrm{H}} \boldsymbol{y}(t)$. Note that the target and the interference sources are in the same/nearby range cell, and the Tx signal $s_{Tx}(t)$ is narrowband. Therefore, similarly to the conventional FDA radar only focusing on the static range-angle dependent beampattern design, we consider an arbitrary $t = t_0$ for the time-varying joint Tx-Rx steering vector $\boldsymbol{a}_J(t; R, \boldsymbol{\delta})$ and perform the matched-filtering operation on the received signal $\bar{y}(t)$ with $s_{Tx}\left(t - \frac{2R_0}{c_0}\right)$ to obtain the following Rx PSFDA output

$$\begin{aligned}\widetilde{y} &= \frac{\int_{T_p} \bar{y}(t) s_{Tx}^*\big(t - \frac{2R_0}{c_0}\big)\, dt}{\int_{T_p} \big|s_{Tx}\big(t - \frac{2R_0}{c_0}\big)\big|^2\, dt} \\ &\approx a_0 \boldsymbol{w}_{Rx}^{\mathrm{H}} \left(\boldsymbol{a}_J(t_0; R_0, \boldsymbol{\delta}_0) \odot \big(\boldsymbol{1}_{2N} \otimes \boldsymbol{w}_{Tx}\big)\right) \\ &\quad + \sum_{k=1}^{K} a_k \boldsymbol{w}_{Rx}^{\mathrm{H}} \big(\boldsymbol{a}_J(t_0; R_k, \boldsymbol{\delta}_k) \odot \big(\boldsymbol{1}_{2N} \otimes \boldsymbol{w}_{Tx}\big)\big) + \widetilde{\xi}, \end{aligned} \tag{21}$$

where the filtered noise $\widetilde{\xi}$ is Gaussian distributed with the zero mean and variance σ_ξ^2. Referring to [30], since the quasi-static steering vector $\boldsymbol{a}_J(t; R_k, \boldsymbol{\delta}_k)$ is available by properly choosing the Tx pulse duration T_p and the frequency offsets $\{\Delta f_1, \Delta f_2\}$, the matched-filtering operation for the conventional FDA radar is still applicable to our work and thus the approximation in (21) is reasonable. According to (21), the output SINR of this proposed polarization-subarray based FDA radar at $t = t_0$ can therefore be expressed as

$$\mathrm{SINR} = \frac{\sigma_0^2 \left| \boldsymbol{w}_{Rx}^{\mathrm{H}} \left(\boldsymbol{a}_J(t_0; R_0, \boldsymbol{\delta}_0) \odot \big(\boldsymbol{1}_{2N} \otimes \boldsymbol{w}_{Tx}\big)\right)\right|^2}{\sum_{k=1}^{K} \sigma_k^2 \left| \boldsymbol{w}_{Rx}^{\mathrm{H}} \left(\boldsymbol{a}_J(t_0; R_k, \boldsymbol{\delta}_k) \odot \big(\boldsymbol{1}_{2N} \otimes \boldsymbol{w}_{Tx}\big)\right)\right|^2 + \sigma_\xi^2}. \tag{22}$$

In the sequel, based on the optimal Tx and Rx beamforming vectors, $\boldsymbol{w}_{Tx}^\star$ and $\boldsymbol{w}_{Rx}^\star$, obtained by maximizing the output SINR (22), the joint Tx-Rx beampattern of our polarization-subarray based FDA radar at $t = t_0$ is designed as

$$B(t_0; R, \boldsymbol{\delta}) = \left| \boldsymbol{w}_{Rx}^{\star \mathrm{H}} \big(\boldsymbol{a}_J(t_0; R, \boldsymbol{\delta}) \odot \big(\boldsymbol{1}_{2N} \otimes \boldsymbol{w}_{Tx}^\star\big)\big)\right|^2. \tag{23}$$

Remark 1: Our generalized PSFDA receiver of Fig. 2 contains both the band-limited coherent PSFDA [31] and the full-band pseudo-coherent PSFDA [31] as two special cases. Specifically, by defining $w_{Rx}^{m,n} = 0$, $\forall n \neq m$ and $n, m = 0, 1, \ldots, 2N-1$, this generalized PSFDA reduces to the band-limited coherent PSFDA, while by defining $w_{Rx}^{m,0} = w_{Rx}^{m,1} = \cdots = w_{Rx}^{m,(2N-1)}$, $\forall m = 0, 1, \ldots, 2N-1$, the full-band pseudo-coherent PSFDA in [31] is obtained. Furthermore, the subarray-based FDA radar of [16] can be considered as a special case of our polarization-subarray based FDA radar. In [16], for all Tx signals with different radiation frequencies from the subarray-based Tx FDA, the corresponding Rx responses of the Rx PA are identical. Mathematically, the system model in [16] corresponds to reformulating $\boldsymbol{B}(\theta, R)$ and $\boldsymbol{p}_e(\boldsymbol{\delta})$ in (17) as $\boldsymbol{B}(\theta, R) = \boldsymbol{B}(\theta) = \mathrm{diag}(\boldsymbol{b}_{fu}(\theta) \otimes \boldsymbol{1}_{2N})$ with

$$\boldsymbol{b}_{fu}(\theta) = \big[1\, e^{\mathrm{j}2\pi k_0 d \sin\theta} \cdots e^{\mathrm{j}2\pi k_0 (2N_r - 1) d \sin\theta}\big]^{\mathrm{T}}, \tag{24}$$

and $\boldsymbol{p}_e(\boldsymbol{\delta}) = c\boldsymbol{1}_{2N}$, where c is a constant. Then based on the full-band pseudo-coherent receiver structure, the signal model of (17) is equivalently reduced to the $2N$-dimensional signal model for the subarray-based FDA radar of [16].

B. Time-Invariant Joint Tx-Rx Beampattern Design

Since the time-dependent joint Tx-Rx beampattern (23) may cause the problem of short target illumination and consequently degrade the target detection performance, we design the time-modulated frequency offset to realize the time-invariant joint Tx-Rx beampattern at the target. To be specific, we extend the time-modulated frequency offset of [20] for realizing time-invariant Tx beampattern of the basic FDA radar to realize the time-invariant spatial focusing beampattern for our polarization-subarray based FDA radar. To this end, we firstly formulate the time-variant phase shift $\bar{\varphi}_{m,n}(t; \theta, R)$ between the $(n+1)$-th antenna of the Tx FDA and the $(m+1)$-th antenna of the Rx PSFDA as given in (25) at the bottom of this page, where $\widetilde{\varphi}_m(\theta) = 2\pi k_0 m d \sin\theta$. Note that $\bar{\varphi}_{m,n}(t; \theta, R)$ corresponds to the $(2Nm + n + 1)$-th element of the joint Tx-Rx steering vector $\boldsymbol{a}_J(t; R, \boldsymbol{\delta})$ given in (20). According to the criterion given in [20], the quadratic phase term $q(m, n)$ in (25), which is

$$\bar{\varphi}_{m,n}(t; \theta, R) = \begin{cases} \widetilde{\varphi}_m(\theta) + 2\pi n \left(\Delta f_1 \left(t - \frac{2R - (m+n) d \sin\theta}{c_0}\right) + k_0 d \sin\theta\right), & n \in \{0, 1, \ldots, N-1\}, \\ \widetilde{\varphi}_m(\theta) + 2\pi (n - N) \left(\Delta f_2 \left(t - \frac{2R - (m+n) d \sin\theta}{c_0}\right) + k_0 d \sin\theta\right), & n \in \{N, N+1, \ldots, 2N-1\}. \end{cases} \tag{25}$$

defined as

$$q(m,n)=\begin{cases}\frac{n(m+n)d\sin\theta\Delta f_1}{c_0}, \\ \quad n\in\{0,1,\ldots,N-1\}, \\ \frac{(n-N)(m+n)d\sin\theta\Delta f_2}{c_0}, \\ \quad n\in\{N,N+1,\ldots,2N-1\},\end{cases} \tag{26}$$

for $m\in\{0,1,\ldots,2N-1\}$, can be ignored when and only when $\left|2\pi q(m,n)\right|\le\frac{\pi}{4}$, $\forall n,m$. Under this condition, we can simplify the phase shift in (25) as

$$\bar{\varphi}_{m,n}(t;\theta,R)\approx \begin{cases}\widetilde{\varphi}_m(\theta)+2\pi n\left(\Delta f_1\left(t-\frac{2R}{c_0}\right)+k_0 d\sin\theta\right), \\ \quad n\in\{0,1,\ldots,N-1\}, \\ \widetilde{\varphi}_m(\theta)+2\pi(n-N)\left(\Delta f_2\left(t-\frac{2R}{c_0}\right)+k_0 d\sin\theta\right), \\ \quad n\in\{N,N+1,\ldots,2N-1\}.\end{cases} \tag{27}$$

Observe from (27) that to achieve the time-invariant beampattern at the target location (θ_0,R_0), the following time modulated frequency offsets $\Delta f_1(t)$ and $\Delta f_2(t)$ can be adopted

$$\begin{cases}\Delta f_1(t)=\frac{l_1-k_0 d\sin\theta_0}{t-\frac{2R_0}{c_0}}, l_1=0,\pm1,\ldots, \\ \Delta f_2(t)=\frac{l_2-k_0 d\sin\theta_0}{t-\frac{2R_0}{c_0}}, l_2=0,\pm1,\ldots,\end{cases} t\in[0,\,T_p]. \tag{28}$$

The specific values of l_1 and l_2 are determined by substituting $\Delta f_1(T_p)$ and $\Delta f_2(T_p)$ into $q(2N-1,N-1)$ and $q(2N-1,2N-1)$, respectively, and considering the constraints

$$\begin{cases}\left|\frac{2\pi(N-1)(3N-2)d\Delta f_1(T_p)}{c_0}\right|\le\frac{\pi}{4}, \\ \left|\frac{2\pi(N-1)(4N-2)d\Delta f_2(T_p)}{c_0}\right|\le\frac{\pi}{4},\end{cases} \tag{29}$$

where $\sin\theta=1$ is implied. According to [30], to realize the quasi-static joint Tx-Rx steering vector $\boldsymbol{a}_J(t;R,\boldsymbol{\delta})$, the values of T_p,l_1 and l_2 should also satisfy $(N-1)\Delta f_1(T_p)T_p\ll1$ and $(N-1)\Delta f_2(T_p)T_p\ll1$. Finally, by substituting (28) into (27) at the arbitrary $t=t_0$, the joint Tx-Rx beampattern (23) at the target location (θ_0,R_0) becomes

$$\begin{aligned}B(t_0;R_0,\boldsymbol{\delta}_0)&=\left|\boldsymbol{w}_{Rx}^{\star\mathrm{H}}\left(\boldsymbol{a}_J(t_0;R_0,\boldsymbol{\delta}_0)\odot(\mathbf{1}_{2N}\otimes\boldsymbol{w}_{Tx}^{\star})\right)\right|^2 \\ &=\left|\boldsymbol{w}_{Rx}^{\star\mathrm{H}}\left(\left(\widetilde{\boldsymbol{P}}_e(\boldsymbol{\delta}_0)\boldsymbol{b}_{fu}(\theta_0)\right)\otimes\boldsymbol{w}_{Tx}^{\star}\right)\right|^2=B(\boldsymbol{\delta}_0).\end{aligned} \tag{30}$$

Clearly, the target beampattern $B(t_0;R_0,\boldsymbol{\delta}_0)$ in (30) is independent of time. Besides, considering the range-angle decoupled characteristics of the subarray-based FDA [16], [17], we conclude that at any time, there exists only a single-maximum and constant joint Tx-Rx beampattern at the target.

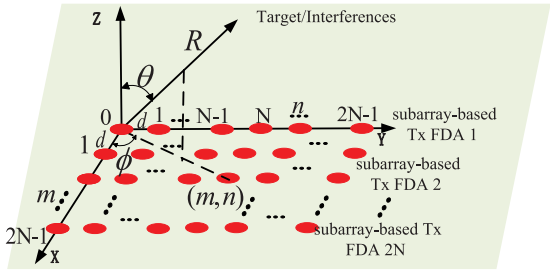

Fig. 3. Illustration of the subarray-based URP FDA transmitter.

C. Output SINR Maximization

Based on the time-invariant beampattern (30) at the target location, the output SINR (22) can be re-expressed as

$$\mathrm{SINR}=\frac{\sigma_0^2\left|\boldsymbol{w}_{Rx}^{\mathrm{H}}\left(\left(\widetilde{\boldsymbol{P}}_e(\boldsymbol{\delta}_0)\boldsymbol{b}_{fu}(\theta_0)\right)\otimes\boldsymbol{w}_{Tx}\right)\right|^2}{\sum_{k=1}^{K}\sigma_k^2\left|\boldsymbol{w}_{Rx}^{\mathrm{H}}\left(\boldsymbol{a}_J(t_0;R_k,\boldsymbol{\delta}_k)\odot\left(\mathbf{1}_{2N_r}\otimes\boldsymbol{w}_{Tx}\right)\right)\right|^2+\sigma_\xi^2}. \tag{31}$$

In order to determine the single-maximum and time-invariant joint Tx-Rx beampattern $B(\boldsymbol{\delta}_0)$ at the target in the presence of interferences, we solve the output SINR maximization problem

$$\begin{aligned}\max_{\boldsymbol{w}_{Rx},\boldsymbol{w}_{Tx},\atop\boldsymbol{P}_e}\ &\frac{\sigma_0^2\left|\boldsymbol{w}_{Rx}^{\mathrm{H}}\left(\left(\widetilde{\boldsymbol{P}}_e(\boldsymbol{\delta}_0)\boldsymbol{b}_{fu}(\theta_0)\right)\otimes\boldsymbol{w}_{Tx}\right)\right|^2}{\sum_{k=1}^{K}\sigma_k^2\left|\boldsymbol{w}_{Rx}^{\mathrm{H}}\left(\boldsymbol{a}_J(t_0;R_k,\boldsymbol{\delta}_k)\odot\left(\mathbf{1}_{2N_r}\otimes\boldsymbol{w}_{Tx}\right)\right)\right|^2+\sigma_\xi^2}, \\ \text{s.t.}\ &\|\boldsymbol{w}_{Rx}\|=1,\ \|\boldsymbol{w}_{Tx}\|=1, \\ &\|\boldsymbol{p}_n\|=1,\ 0\le n\le 2N-1.\end{aligned} \tag{32}$$

Unfortunately, the problem (32) is nonconvex and generally intractable due to the nonlinearly coupled optimization variables. To overcome this difficulty, an alternating suboptimal algorithm is proposed to optimize the FDA Tx beamforming $\boldsymbol{w}_{Tx}$, the PSFDA Rx beamforming $\boldsymbol{w}_{Rx}$ and the PSFDA spatial pointing matrix $\boldsymbol{P}_e$ iteratively in Section III.

D. Extension to Polarization-Subarray URP FDA Radar

We now discuss how to extend the proposed joint Tx-Rx steering vector and the beampattern design for the polarization-subarray based UL FDA radar to the URP FDA radar, which can facilitate the three-dimensional beamforming in both elevation and azimuth domains, and thus improve target localization accuracy and efficiently mitigate the interferences. As shown in Fig. 3, the subarray-based Tx URP FDA consists of $2N$ parallel subarray-based UL Tx FDAs, which are uniformly placed in the vertical X-axis direction with the inter-array spacing d. Similarly, the Rx URP PSFDA is also composed of $2N$ parallel UL PSFDAs, uniformly placed in the vertical X-axis direction. Then we can reformulate the Tx beamforming $\boldsymbol{w}_{Tx,P}\in\mathbb{C}^{4N^2}$ and steering vector $\boldsymbol{a}_P(t;\theta,\phi,R)\in\mathbb{C}^{4N^2}$ at the spatial location (θ,ϕ,R) of the subarray-based Tx URP FDA as

$$\boldsymbol{w}_{Tx,P}=\left[w_{Tx}^{0,0}\cdots w_{Tx}^{0,L}\cdots w_{Tx}^{L,0}\cdots w_{Tx}^{L,L}\right]^{\mathrm{T}}, \tag{33}$$

$$\boldsymbol{a}_P(t;\theta,\phi,R)=\left[e^{\mathrm{j}\varphi_{0,0}(t)}\cdots e^{\mathrm{j}\varphi_{m,n}(t)}\cdots e^{\mathrm{j}\varphi_{L,L}(t)}\right]^{\mathrm{T}}, \tag{34}$$

where $L = 2N - 1$. In (34), $\varphi_{m,n}(t)$ is the phase shift between the (m,n)-th Tx antenna element in the vertical-horizontal $(X-Y)$ plane and the spatial location (θ, ϕ, R), given by

$$\varphi_{m,n}(t) = \begin{cases} 2\pi k_0 d_{m,n} + 2\pi m \Delta f_1 (t - \tau_{m,n}), \\ \quad n \in \{0, 1, \ldots, N-1\}, \\ 2\pi k_0 d_{m,n} + 2\pi (m-N) \Delta f_2 (t - \tau_{m,n}), \\ \quad n \in \{N, N+1, \ldots, L\}, \end{cases} \tag{35}$$

for $m \in \{0, 1, \ldots, 2N-1\}$, where $d_{m,n} = d(m \sin\theta \cos\phi + n \sin\theta \sin\phi)$ and $\tau_{m,n} = \frac{R - d_{m,n}}{c_0}$.

Similarly to the derivation of the $4N^2$ dimensional received signal (17) for the Rx UL PSFDA, by considering the full-band reception as that in Fig. 2 and the polarization sensitivity of the Rx URP PSFDA, we can also model the $16N^4$-dimensional steering vector $\boldsymbol{b}(\theta, \phi, R)$ of the Rx URP PSFDA as

$$\boldsymbol{b}(\theta, \phi, R) = \left[\boldsymbol{b}_{0,0}^{\mathrm{T}} \cdots \boldsymbol{b}_{0,L}^{\mathrm{T}} \cdots \boldsymbol{b}_{m_1,n_1}^{\mathrm{T}} \cdots \boldsymbol{b}_{L,0}^{\mathrm{T}} \cdots \boldsymbol{b}_{L,L}^{\mathrm{T}}\right]^{\mathrm{T}}, \tag{36}$$

with

$$\boldsymbol{b}_{m_1,n_1} = \left[e^{\mathrm{j}b_{m_1,n_1}^{0,0}} \cdots e^{\mathrm{j}b_{m_1,n_1}^{m,n}} \cdots e^{\mathrm{j}b_{m_1,n_1}^{L,L}}\right]^{\mathrm{T}} \in \mathbb{C}^{4N^2} \tag{37}$$

$$b_{m_1,n_1}^{m,n} = \begin{cases} 2\pi k_0 d_{m_1,n_1} - 2\pi n \Delta f_1 \tau_{m_1,n_1}, \\ \quad n \in \{0, 1, \ldots, N-1\}, \\ 2\pi k_0 d_{m_1,n_1} - 2\pi (n-N) \Delta f_2 \tau_{m_1,n_1}, \\ \quad n \in \{N, N+1, \ldots, L\}, \end{cases} \tag{38}$$

for $m \in \{0, 1, \ldots, L\}$ and $m_1, n_1 \in \{0, 1, \ldots, L\}$. Here, the (m_1, n_1)-th Rx antenna element is located in the vertical-horizontal plane. Then we can formulate the $16N^4$-dimensional baseband received signal at the Rx URP PSFDA as given in (39) at the bottom of this page, where

$$\widetilde{\boldsymbol{P}}_{e,pl}(\boldsymbol{\delta}) = \mathrm{diag}\big(\boldsymbol{p}_{e,pl}(\boldsymbol{\delta})\big) \in \mathbb{C}^{4N^2 \times 4N^2}, \tag{40}$$

$$\boldsymbol{p}_{e,pl}(\boldsymbol{\delta}) = \boldsymbol{P}_{e,pl}\boldsymbol{e}(\boldsymbol{\delta}) \in \mathbb{C}^{4N^2}, \tag{41}$$

$$\boldsymbol{P}_{e,pl} = G_e \left[\boldsymbol{p}_{0,0}^{\mathrm{T}} \cdots \boldsymbol{p}_{0,L}^{\mathrm{T}} \cdots \boldsymbol{p}_{L,0}^{\mathrm{T}} \cdots \boldsymbol{p}_{L,L}^{\mathrm{T}}\right]^{\mathrm{T}} \in \mathbb{R}^{4N^2 \times 3}, \tag{42}$$

$$\boldsymbol{A}_P(t; \theta, \phi, R) = \mathrm{diag}(\boldsymbol{a}_P(t; \theta, \phi, R)) \in \mathbb{C}^{4N^2 \times 4N^2}, \tag{43}$$

where $\boldsymbol{P}_{e,pl}$ is the spatial pointing matrix of the Rx URP PSFDA, and similarly defined as in (12) and (13). From (39), the joint Tx-Rx steering vector of the polarization-subarray based URP FDA radar is given by

$$\boldsymbol{a}_{J,P}(t; R, \boldsymbol{\delta}) = \left(\widetilde{\boldsymbol{P}}_{e,pl}(\boldsymbol{\delta}) \otimes \boldsymbol{A}_P(t; \theta, \phi, R)\right) \boldsymbol{b}(\theta, \phi, R). \tag{44}$$

Furthermore, we can define the unit-norm Rx beamforming $\boldsymbol{w}_{Rx,P} \in \mathbb{C}^{16N^4}$ of the Rx URP PSFDA as

$$\boldsymbol{w}_{Rx,P} = \left[\left(\boldsymbol{w}_{Rx,P}^{0,0}\right)^{\mathrm{T}} \cdots \left(\boldsymbol{w}_{Rx,P}^{m_1,n_1}\right)^{\mathrm{T}} \cdots \left(\boldsymbol{w}_{Rx,P}^{L,L}\right)^{\mathrm{T}}\right]^{\mathrm{T}}, \tag{45}$$

$$\boldsymbol{w}_{Rx,P}^{m_1,n_1} = \left[w_{Rx,P}^{m_1,n_1,0,0} \cdots w_{Rx}^{m_1,n_1,m,n} \cdots w_{Rx}^{m_1,n_1,L,L}\right] \in \mathbb{C}^{4N^2}. \tag{46}$$

Similarly, after the matched-filtering operation and by fixing $t = t_0$ in $\boldsymbol{a}_{J,P}(t; R, \boldsymbol{\delta})$, the output SINR of the polarization-subarray based URP FDA radar is expressed as

$$\mathrm{SINR} = \frac{\sigma_0^2 \left|\boldsymbol{w}_{Rx,P}^{\mathrm{H}} \left(\boldsymbol{a}_{J,P}(t_0; R_0, \boldsymbol{\delta}_0) \odot \left(\boldsymbol{1}_{4N^2} \otimes \boldsymbol{w}_{Tx,P}\right)\right)\right|^2}{\sum_{k=1}^{K} \sigma_k^2 \left|\boldsymbol{w}_{Rx,P}^{\mathrm{H}} \left(\boldsymbol{a}_{J,P}(t_0; R_k, \boldsymbol{\delta}_k) \odot \left(\boldsymbol{1}_{4N^2} \otimes \boldsymbol{w}_{Tx,P}\right)\right)\right|^2 + \sigma_\xi^2}. \tag{47}$$

Once the optimal Tx and Rx beamforming vectors, $\boldsymbol{w}_{Rx,P}^{\star}$ and $\boldsymbol{w}_{Tx,P}^{\star}$, are derived, the corresponding joint Tx-Rx beampattern at $t = t_0$ is given by

$$B_P(t_0; R, \boldsymbol{\delta}) = \left|\boldsymbol{w}_{Rx,P}^{\star \mathrm{H}} \left(\boldsymbol{a}_{J,P}(t_0; R_0, \boldsymbol{\delta}_0) \odot \left(\boldsymbol{1}_{4N^2} \otimes \boldsymbol{w}_{Tx,P}^{\star}\right)\right)\right|^2. \tag{48}$$

For the polarization-subarray based URP FDA radar, we clearly find that the joint Tx-Rx steering vector in (44), the output SINR in (47) and the joint Tx-Rx beampattern in (48) have the similar structures to those of (20), (22) and (23) for the polarization-subarray based UL FDA radar, respectively. Therefore, we readily infer that both the time-invariant joint Tx-Rx beampattern design given in Section II-B and the alternating optimization proposed in Section III for the output SINR maximization problem (32) are applicable to this URP FDA radar. This extension is straightforward.

III. Proposed Alternating Optimization Algorithm

As mentioned previously, it is challenging to obtain the jointly optimal FDA Tx beamforming $\boldsymbol{w}_{Tx}^{\star}$, PSFDA Rx beamforming $\boldsymbol{w}_{Rx}^{\star}$ and PSFDA spatial pointing matrix $\boldsymbol{P}_e^{\star}$ for the optimization problem (32). In this section, we detail our proposed suboptimal alternating algorithm, which iteratively optimizes $\boldsymbol{w}_{Tx}$, $\boldsymbol{w}_{Rx}$ and $\boldsymbol{P}_e$. Moreover, the adaptive realization of the joint Tx-Rx beampattern design based on the proposed alternating algorithm is also briefly introduced.

$$\begin{aligned} \boldsymbol{y}_P(t) = a_0 \underbrace{\left(\left(\widetilde{\boldsymbol{P}}_{e,pl}(\boldsymbol{\delta}_0) \otimes \boldsymbol{A}_P(t; \theta_0, \phi_0, R_0)\right)\boldsymbol{b}(\theta_0, \phi_0, R_0)\right)}_{\boldsymbol{a}_{J,P}(t; R_0, \boldsymbol{\delta}_0)} \odot \left(\boldsymbol{1}_{4N^2} \otimes \boldsymbol{w}_{Tx,P}\right) s_{Tx}\left(t - \frac{2R_0}{c_0}\right) \\ + \sum_{k=1}^{K} a_k \underbrace{\left(\left(\widetilde{\boldsymbol{P}}_{e,pl}(\boldsymbol{\delta}_k) \otimes \boldsymbol{A}_P(t; \theta_k, \phi_k, R_k)\right)\boldsymbol{b}(\theta_k, \phi_k, R_k)\right)}_{\boldsymbol{a}_{J,P}(t; R_k, \boldsymbol{\delta}_k)} \odot \left(\boldsymbol{1}_{4N^2} \otimes \boldsymbol{w}_{Tx,P}\right) s_{Tx}\left(t - \frac{2R_k}{c_0}\right) + \boldsymbol{\xi}(t), \end{aligned} \tag{39}$$

A. Optimization of FDA Tx Beamforming $\boldsymbol{w}_{Tx}$

When the PSFDA Rx beamforming $\boldsymbol{w}_{Rx}$ and the spatial pointing matrix $\boldsymbol{P}_e$ are fixed, after a tedious but straightforward derivation, the optimization problem (32) w.r.t. the FDA Tx beamforming $\boldsymbol{w}_{Tx}$ can be reformulated as

$$\max_{\boldsymbol{w}_{Tx}} \frac{\sigma_0^2 \boldsymbol{w}_{Tx}^{\mathrm{H}} \widetilde{\boldsymbol{f}}_0 \widetilde{\boldsymbol{f}}_0^{\mathrm{H}} \boldsymbol{w}_{Tx}}{\boldsymbol{w}_{Tx}^{\mathrm{H}} \left(\sigma_\xi^2 \boldsymbol{I}_{2N} + \sum_{k=1}^{K} \sigma_k^2 \widetilde{\boldsymbol{f}}_k(t_0) \widetilde{\boldsymbol{f}}_k^{\mathrm{H}}(t_0)\right) \boldsymbol{w}_{Tx}}, \quad (49)$$

where the auxiliary variables $\widetilde{\boldsymbol{f}}_0 \in \mathbb{C}^{2N}$ and $\widetilde{\boldsymbol{f}}_k(t_0) \in \mathbb{C}^{2N}$ for $1 \le k \le K$ are defined respectively as

$$\widetilde{\boldsymbol{f}}_0 = \boldsymbol{\Lambda}_P^{[0]} \boldsymbol{w}_{Rx}, \quad (50)$$

with

$$\boldsymbol{\Lambda}_P^{[0]} = \left[\boldsymbol{\Lambda}_{P,1}^{[0]}\, \boldsymbol{\Lambda}_{P,2}^{[0]} \cdots \boldsymbol{\Lambda}_{P,2N}^{[0]}\right] \in \mathbb{C}^{2N \times 4N^2}, \quad (51)$$

$$\boldsymbol{\Lambda}_{P,i}^{[0]} = \left(\widetilde{\boldsymbol{P}}_e(\boldsymbol{\delta}_0)\boldsymbol{b}_{fu}(\theta_0)\right)|_{[i:i]} \boldsymbol{I}_{2N} \in \mathbb{C}^{2N \times 2N}, 1 \le i \le 2N, \quad (52)$$

and

$$\widetilde{\boldsymbol{f}}_k(t_0) = \boldsymbol{\Lambda}_P^{[k]}(t_0) \boldsymbol{w}_{Rx},\ 1 \le k \le K, \quad (53)$$

with

$$\boldsymbol{\Lambda}_P^{[k]}(t_0) = \left[\boldsymbol{\Lambda}_{P,1}^{[k]}(t_0) \cdots \boldsymbol{\Lambda}_{P,2N}^{[k]}(t_0)\right] \in \mathbb{C}^{2N \times 4N^2}, \quad (54)$$

$$\boldsymbol{\Lambda}_{P,i}^{[k]}(t_0) = \mathrm{diag}\Big(\boldsymbol{a}_J(t_0; R_k, \boldsymbol{\delta}_k)|_{[2N(i-1)+1:2Ni]}\Big) \in \mathbb{C}^{2N \times 2N}, \quad 1 \le i \le 2N. \quad (55)$$

The optimization (49) is a standard generalized Rayleigh quotient problem [32] w.r.t. the FDA Tx beamforming vector $\boldsymbol{w}_{Tx}$. As a result, the optimal FDA Tx beamforming is the generalized eigenvector corresponding to the largest generalized eigenvalue of the matrix pencil $\left(\bar{\boldsymbol{F}}_0, \bar{\boldsymbol{F}}_1(t_0)\right)$, where

$$\bar{\boldsymbol{F}}_0 = \widetilde{\boldsymbol{f}}_0 \widetilde{\boldsymbol{f}}_0^{\mathrm{H}} \in \mathbb{C}^{2N \times 2N}, \quad (56)$$

$$\bar{\boldsymbol{F}}_1(t_0) = \sigma_\xi^2 \boldsymbol{I}_{2N} + \sum_{k=1}^{K} \sigma_k^2 \widetilde{\boldsymbol{f}}_k(t_0) \widetilde{\boldsymbol{f}}_k^{\mathrm{H}}(t_0) \in \mathbb{C}^{2N \times 2N}. \quad (57)$$

Since $\bar{\boldsymbol{F}}_1(t_0)$ is nonsingular, the optimal $\widehat{\boldsymbol{w}}_{Tx}^{\star}$ to the problem (49) is also the normalized eigenvector associated with the maximum eigenvalue of $\bar{\boldsymbol{F}}_1^{-1}(t_0)\bar{\boldsymbol{F}}_0$

$$\widehat{\boldsymbol{w}}_{Tx}^{\star} = \boldsymbol{\vartheta}\left(\bar{\boldsymbol{F}}_1^{-1}(t_0)\bar{\boldsymbol{F}}_0\right), \quad (58)$$

where $\boldsymbol{\vartheta}(\boldsymbol{A})$ is the unit-norm eigenvector corresponding to the maximum eigenvalue $\lambda_{\max}(\boldsymbol{A})$ of a square matrix $\boldsymbol{A}$. Considering that $\bar{\boldsymbol{F}}_0$ is rank-1, $\bar{\boldsymbol{F}}_1^{-1}(t_0)\bar{\boldsymbol{F}}_0$ is also rank-1 and only has one nonzero eigenvalue. Thus we have

$$\left[\bar{\boldsymbol{F}}_1^{-1}(t_0)\bar{\boldsymbol{F}}_0\right]\left[\bar{\boldsymbol{F}}_1^{-1}(t_0)\widetilde{\boldsymbol{f}}_0\right] = \left[\bar{\boldsymbol{F}}_1^{-1}(t_0)\widetilde{\boldsymbol{f}}_0\widetilde{\boldsymbol{f}}_0^{\mathrm{H}}\right]\left[\bar{\boldsymbol{F}}_1^{-1}(t_0)\widetilde{\boldsymbol{f}}_0\right] = \left[\widetilde{\boldsymbol{f}}_0^{\mathrm{H}}\bar{\boldsymbol{F}}_1^{-1}(t_0)\widetilde{\boldsymbol{f}}_0\right]\left[\bar{\boldsymbol{F}}_1^{-1}(t_0)\widetilde{\boldsymbol{f}}_0\right], \quad (59)$$

based on which, the nonzero eigenvalue and the corresponding normalized eigenvector of $\bar{\boldsymbol{F}}_1^{-1}(t_0)\bar{\boldsymbol{F}}_0$ are

$$\lambda_{\max}\left(\bar{\boldsymbol{F}}_1^{-1}(t_0)\bar{\boldsymbol{F}}_0\right) = \widetilde{\boldsymbol{f}}_0^{\mathrm{H}}\bar{\boldsymbol{F}}_1^{-1}(t_0)\widetilde{\boldsymbol{f}}_0, \quad (60)$$

$$\boldsymbol{\vartheta}\left(\bar{\boldsymbol{F}}_1^{-1}(t_0)\bar{\boldsymbol{F}}_0\right) = \frac{\bar{\boldsymbol{F}}_1^{-1}(t_0)\widetilde{\boldsymbol{f}}_0}{\left\|\bar{\boldsymbol{F}}_1^{-1}(t_0)\widetilde{\boldsymbol{f}}_0\right\|}. \quad (61)$$

Thus the optimal $\widehat{\boldsymbol{w}}_{Tx}^{\star}$ to the problem (49) is

$$\widehat{\boldsymbol{w}}_{Tx}^{\star} = \frac{\bar{\boldsymbol{F}}_1^{-1}(t_0)\widetilde{\boldsymbol{f}}_0}{\left\|\bar{\boldsymbol{F}}_1^{-1}(t_0)\widetilde{\boldsymbol{f}}_0\right\|}. \quad (62)$$

B. Optimization of PSFDA Rx Beamforming $\boldsymbol{w}_{Rx}$

When $\boldsymbol{w}_{Tx}$ and $\boldsymbol{P}_e$ are given, the SINR maximization problem (32) can also be reduced to a generalized Rayleigh quotient problem w.r.t. the PSFDA Rx beamforming $\boldsymbol{w}_{Rx}$. Specifically, we can define the auxiliary variables $\boldsymbol{g}_0 \in \mathbb{C}^{4N^2}$ and $\boldsymbol{g}_k(t_0) \in \mathbb{C}^{4N^2}$ for $1 \le k \le K$, respectively, as

$$\boldsymbol{g}_0 = \left(\widetilde{\boldsymbol{P}}_e(\boldsymbol{\delta}_0)\boldsymbol{b}_{fu}(\theta_0)\right) \otimes \boldsymbol{w}_{Tx}, \quad (63)$$

$$\boldsymbol{g}_k(t_0) = \boldsymbol{a}_J(t_0; R_k, \boldsymbol{\delta}_k) \odot \left(\boldsymbol{1}_{2N} \otimes \boldsymbol{w}_{Tx}\right). \quad (64)$$

By further defining the following matrices

$$\bar{\boldsymbol{\Lambda}}_0 = \boldsymbol{g}_0\boldsymbol{g}_0^{\mathrm{H}} \in \mathbb{C}^{4N^2 \times 4N^2}, \quad (65)$$

$$\bar{\boldsymbol{\Lambda}}_1(t_0) = \left(\sigma_\xi^2 \boldsymbol{I}_{4N^2} + \sum_{k=1}^{K} \sigma_k^2 \boldsymbol{g}_k(t_0)\boldsymbol{g}_k^{\mathrm{H}}(t_0)\right) \in \mathbb{C}^{4N^2 \times 4N^2}, \quad (66)$$

we have the reformulated problem (32) w.r.t. $\boldsymbol{w}_{Rx}$ as

$$\max_{\boldsymbol{w}_{Rx}} \frac{\sigma_0^2 \boldsymbol{w}_{Rx}^{\mathrm{H}} \bar{\boldsymbol{\Lambda}}_0 \boldsymbol{w}_{Rx}}{\boldsymbol{w}_{Rx}^{\mathrm{H}} \bar{\boldsymbol{\Lambda}}_1(t_0) \boldsymbol{w}_{Rx}}. \quad (67)$$

Similarly to the problem (49), the optimal $\widehat{\boldsymbol{w}}_{Rx}^{\star}$ is a normalized eigenvector corresponding to the largest eigenvalue of the matrix pencil $\left(\bar{\boldsymbol{\Lambda}}_0, \bar{\boldsymbol{\Lambda}}_1(t_0)\right)$. Since $\bar{\boldsymbol{\Lambda}}_1(t_0)$ is nonsingular and the rank of $\bar{\boldsymbol{\Lambda}}_0$ is one, the optimal PSFDA Rx beamforming $\widehat{\boldsymbol{w}}_{Rx}^{\star}$ is also the normalized eigenvector associated with the single nonzero eigenvalue of $\bar{\boldsymbol{\Lambda}}_i^{-1}(t_0)\bar{\boldsymbol{\Lambda}}_0$. By noting

$$\left[\bar{\boldsymbol{\Lambda}}_1^{-1}(t_0)\bar{\boldsymbol{\Lambda}}_0\right]\left[\bar{\boldsymbol{\Lambda}}_1^{-1}(t_0)\boldsymbol{g}_0\right] = \left[\bar{\boldsymbol{\Lambda}}_1^{-1}(t_0)\boldsymbol{g}_0\boldsymbol{g}_0^{\mathrm{H}}\right]\left[\bar{\boldsymbol{\Lambda}}_1^{-1}(t_0)\boldsymbol{g}_0\right] = \left[\boldsymbol{g}_0^{\mathrm{H}}\bar{\boldsymbol{\Lambda}}_1^{-1}(t_0)\boldsymbol{g}_0\right]\left[\bar{\boldsymbol{\Lambda}}_1^{-1}(t_0)\boldsymbol{g}_0\right], \quad (68)$$

we readily have $\lambda_{\max}\left(\bar{\boldsymbol{\Lambda}}_1^{-1}(t_0)\bar{\boldsymbol{\Lambda}}_0\right) = \boldsymbol{g}_0^{\mathrm{H}}\bar{\boldsymbol{\Lambda}}_1^{-1}(t_0)\boldsymbol{g}_0$ and $\boldsymbol{\vartheta}\left(\bar{\boldsymbol{\Lambda}}_1^{-1}(t_0)\bar{\boldsymbol{\Lambda}}_0\right) = \frac{\bar{\boldsymbol{\Lambda}}_1^{-1}(t_0)\boldsymbol{g}_0}{\|\bar{\boldsymbol{\Lambda}}_1^{-1}(t_0)\boldsymbol{g}_0\|}$. Thus the optimal $\widehat{\boldsymbol{w}}_{Rx}^{\star}$ to the problem (67) is derived as

$$\widehat{\boldsymbol{w}}_{Rx}^{\star} = \frac{\bar{\boldsymbol{\Lambda}}_1^{-1}(t_0)\boldsymbol{g}_0}{\left\|\bar{\boldsymbol{\Lambda}}_1^{-1}(t_0)\boldsymbol{g}_0\right\|}. \quad (69)$$

C. Optimization of PSFDA Spatial Pointings $\boldsymbol{P}_e$

Given the FDA Tx beamforming $\boldsymbol{w}_{Tx}$ and the PSFDA Rx beamforming $\boldsymbol{w}_{Rx}$, we can transform the problem (32) into the following optimization problem w.r.t. the PSFDA spatial

pointings $\boldsymbol{P}_e$

$$\begin{aligned}&\max_{\bar{\boldsymbol{p}}_e} \frac{\sigma_0^2\left|\bar{\boldsymbol{p}}_e^{\mathrm{T}}\boldsymbol{u}_0\right|^2}{\sigma_\xi^2+\sum_{k=1}^K\sigma_k^2\left|\bar{p}_e^{\mathrm{T}}u_k(t_0)\right|^2},\\ &\text{s.t. } \left\|\bar{\boldsymbol{p}}_e|_{[3n+1:3n+3]}\right\|=\|\boldsymbol{p}_n\|=1, 0\le n\le 2N-1,\end{aligned} \tag{70}$$

where the spatial pointing vector $\boldsymbol{p}_n\in\mathbb{R}^{1\times 3}$ is given in (13), and we have

$$\bar{\boldsymbol{p}}_e=\left[\boldsymbol{p}_0\,\boldsymbol{p}_1\cdots\boldsymbol{p}_{2N-1}\right]^{\mathrm{T}}\in\mathbb{R}^{6N}, \tag{71}$$

$$\boldsymbol{u}_0=\left(\mathrm{diag}\big(\boldsymbol{b}_{fu}(\theta_0)\big)\bar{\boldsymbol{w}}_{Rx}^{\mathrm{H}}\boldsymbol{w}_{Tx}\right)\otimes\boldsymbol{e}(\boldsymbol{\delta}_0)\in\mathbb{C}^{6N}, \tag{72}$$

with

$$\bar{\boldsymbol{w}}_{Rx}=\left[\boldsymbol{w}_{Rx}^{[0]}\,\boldsymbol{w}_{Rx}^{[1]}\cdots\boldsymbol{w}_{Rx}^{[2N-1]}\right]\in\mathbb{C}^{2N\times 2N}, \tag{73}$$

$$\boldsymbol{w}_{Rx}^{[i]}=\boldsymbol{w}_{Rx}|_{[2Ni+1:2N(i+1)]}\in\mathbb{C}^{2N}, 0\le i\le 2N-1, \tag{74}$$

as well as

$$\boldsymbol{u}_k(t_0)=(\boldsymbol{I}_{2N}\otimes\boldsymbol{e}(\boldsymbol{\delta}_k))\bar{\boldsymbol{B}}_k\left(\boldsymbol{I}_{2N}\otimes\boldsymbol{A}^{\mathrm{H}}(t_0;\theta_k,R_k)\right)\boldsymbol{w}_{Rx}\in\mathbb{C}^{6N}, \tag{75}$$

with

$$\bar{\boldsymbol{b}}_k=\boldsymbol{b}(\theta_k,R_k)\odot(\boldsymbol{1}_{2N}\otimes\boldsymbol{w}_{Tx})\in\mathbb{C}^{4N^2}, \tag{76}$$

$$\bar{\boldsymbol{b}}_k^{[i]}=\bar{\boldsymbol{b}}_k^*|_{[2Ni+1:2N(i+1)]}\in\mathbb{C}^{2N},\ 0\le i\le 2N-1, \tag{77}$$

$$\bar{\boldsymbol{B}}_k=\left[\mathrm{diag}\big(\bar{\boldsymbol{b}}_k^{[0]}\big)\cdots\mathrm{diag}\big(\bar{\boldsymbol{b}}_k^{[2N-1]}\big)\right]\in\mathbb{C}^{2N\times 4N^2}. \tag{78}$$

However, the problem (70) is nonconvex because of the nonlinear optimization objective. To effectively solve the problem (70), we first convert it to a standard semidefinite programming (SDP) problem with a rank-1 constraint by defining the following Hermitian matrix

$$\breve{\boldsymbol{P}}_e=\bar{\boldsymbol{p}}_e^*\bar{\boldsymbol{p}}_e^{\mathrm{T}}\in\mathbb{R}^{6N\times 6N}, \tag{79}$$

of which the rank-1 property, i.e., $\mathrm{rank}\big(\breve{\boldsymbol{P}}_e\big)=1$, is implied. Then the problem (70) is reformulated as

$$\begin{aligned}&\max_{\bar{\boldsymbol{P}}_e}\ \frac{\sigma_0^2\mathrm{Tr}\big(\breve{\boldsymbol{P}}_e\boldsymbol{D}_0\big)}{\sigma_\xi^2+\sum_{k=1}^K\sigma_k^2\mathrm{Tr}\big(\breve{\boldsymbol{P}}_e\boldsymbol{D}_k\big)},\\ &\text{s.t. } \mathrm{Tr}\big(\breve{\boldsymbol{P}}_e\breve{\boldsymbol{I}}_n\big)=1,\ 0\le n\le 2N-1,\\ &\qquad\breve{\boldsymbol{P}}_e\succeq\boldsymbol{0},\ \mathrm{rank}\big(\breve{\boldsymbol{P}}_e\big)=1,\end{aligned} \tag{80}$$

where $\boldsymbol{D}_0=\boldsymbol{u}_0\boldsymbol{u}_0^{\mathrm{H}}\in\mathbb{C}^{6N\times 6N}$, $\boldsymbol{D}_k=\boldsymbol{u}_k(t_0)\boldsymbol{u}_k^{\mathrm{H}}(t_0)\in\mathbb{C}^{6N\times 6N}$ for $1\le k\le K$, and $\breve{\boldsymbol{I}}_n=\widetilde{\boldsymbol{I}}_n^{\mathrm{H}}\widetilde{\boldsymbol{I}}_n\in\mathbb{C}^{6N\times 6N}$ with $\widetilde{\boldsymbol{I}}_n=\left[\boldsymbol{0}_{3\times 3n}\,\boldsymbol{I}_3\,\boldsymbol{0}_{3\times 3(2N-n-1)}\right]\in\mathbb{C}^{3\times 6N}$. By further introducing the auxiliary variable

$$\bar{\boldsymbol{P}}_e=\eta\breve{\boldsymbol{P}}_e, \tag{81}$$

with

$$\eta=\frac{\sigma_0^2}{\sigma_\xi^2+\sum_{k=1}^K\sigma_k^2\mathrm{Tr}\big(\breve{\boldsymbol{P}}_e\boldsymbol{D}_k\big)}, \tag{82}$$

and performing the Charnes-Cooper transformation [33] on the problem (80), we equivalently transform the problem (80) to

$$\begin{aligned}&\max_{\bar{\boldsymbol{P}}_e,\eta}\ \mathrm{Tr}\left(\bar{\boldsymbol{P}}_e\boldsymbol{D}_0\right),\\ &\text{s.t. }\sum_{k=1}^K\sigma_k^2\mathrm{Tr}\left(\bar{\boldsymbol{P}}_e\boldsymbol{D}_k\right)+\eta\sigma_\xi^2=\sigma_0^2,\\ &\qquad\mathrm{Tr}\left(\bar{\boldsymbol{P}}_e\breve{\boldsymbol{I}}_n\right)=\eta,\ 0\le n\le 2N-1,\\ &\qquad\bar{\boldsymbol{P}}_e\succeq\boldsymbol{0},\ \mathrm{rank}\big(\bar{\boldsymbol{P}}_e\big)=1.\end{aligned} \tag{83}$$

Unfortunately, the problem (83) is still nonconvex due to the coupled variables and the rank-1 constraint on $\bar{\boldsymbol{P}}_e$, and a direct optimization is generally difficult to conduct. Therefore, we propose applying the semidefinite relaxation (SDR) method to solve the problem (83) effectively. Specifically, by neglecting the rank-1 constraint, the optimization problem (83) becomes a standard SDP problem. If the obtained $\bar{\boldsymbol{P}}_e$ by solving the relaxed (83) satisfies the rank-1 constraint, the optimal $\bar{\boldsymbol{p}}_e$ can be computed by performing the eigenvalue decomposition and thus the corresponding optimal PSFDA spatial pointing matrix $\boldsymbol{P}_e^\star$ is derived through the matrix reshaping operation. Otherwise, for the obtained $\bar{\boldsymbol{P}}_e$ that does not satisfy the rank-1 constraint, a randomization method is utilized to generate a large number of candidates $\bar{\boldsymbol{p}}_e$ whose covariance matrices are all equal to $\bar{\boldsymbol{P}}_e/\eta$, and we always pick the proximate one that satisfies all the constraints of (70). However, due to the fact that the search space is generally finite and random, it is possible that a rank-1 solution satisfying all the constraints of the optimization problem (70) does not exist.

To tackle this potential non rank-1 solution difficulty, the penalty function method proposed in [32] is applied. In fact, the penalty function method is based on the following inequality for the semi-positive definite matrix $\bar{\boldsymbol{P}}_e$

$$\mathrm{Tr}\big(\bar{\boldsymbol{P}}_e\big)-\lambda_{\max}\big(\bar{\boldsymbol{P}}_e\big)\ge 0, \tag{84}$$

where the equality holds for the rank-1 $\bar{\boldsymbol{P}}_e$. Therefore, by substituting the left-hand function of the inequality (84), i.e., $\mathrm{Tr}\big(\bar{\boldsymbol{P}}_e\big)-\lambda_{\max}\big(\bar{\boldsymbol{P}}_e\big)$, into the optimization objective of the problem (83), we can obtain the rank-1 satisfied $\bar{\boldsymbol{P}}_e$ to the problem (83) by iteratively solving the resultant minimization problem. This iterative process has been proved to converge to a locally optimal and rank-1 satisfied solution $\bar{\boldsymbol{P}}_e$ in [32]. Specifically, at the t-th iteration, given $\bar{\boldsymbol{P}}_e^{(t-1)}$ obtained at the previous iteration, we solve the following optimization problem to obtain the rank-1 asymptotic solution $\bar{\boldsymbol{P}}_e^{(t)}$

$$\begin{aligned}&\min_{\bar{\boldsymbol{P}}_e,\eta}\ \mathrm{Tr}\left(\big(\boldsymbol{I}_{6N}-\boldsymbol{D}_0\big)\bar{\boldsymbol{P}}_e\right)-\lambda_{\max}\left(\bar{\boldsymbol{P}}_e^{(t-1)}\right)\\ &\qquad-\mathrm{Tr}\left(\boldsymbol{v}_{\max}^{(t-1)}\big(\boldsymbol{v}_{\max}^{(t-1)}\big)^{\mathrm{H}}\big(\bar{\boldsymbol{P}}_e-\bar{\boldsymbol{P}}_e^{(t-1)}\big)\right),\\ &\text{s.t. }\sum_{k=1}^K\sigma_k^2\mathrm{Tr}\left(\bar{\boldsymbol{P}}_e\boldsymbol{D}_k\right)+\eta\sigma_\xi^2=\sigma_0^2,\\ &\qquad\bar{\boldsymbol{P}}_e\succeq\boldsymbol{0},\ \mathrm{Tr}\left(\bar{\boldsymbol{P}}_e\breve{\boldsymbol{I}}_n\right)=\eta,\ 0\le n\le 2N-1,\end{aligned} \tag{85}$$

where $\boldsymbol{v}_{\max}^{(t-1)}$ is the normalized eigenvector corresponding to the maximum eigenvalue of the matrix $\bar{\boldsymbol{P}}_e^{(t-1)}$. Clearly, the

Algorithm 1: Penalty Function Method for Obtaining $\widehat{\boldsymbol{P}}_e^{\star}$.

Initialize: Give $\boldsymbol{w}_{Tx}$ and $\boldsymbol{w}_{Rx}$; Set iteration index $I_{inn}=0$;

1: Solve the problem (83) minus its rank-1 constraint to obtain initial $\bar{\boldsymbol{P}}_e^{(I_{inn})}$ for the optimization (85);
2: **repeat**
3: $I_{inn}=I_{inn}+1$;
4: Solve the problem (85) for given $\bar{\boldsymbol{P}}_e^{(I_{inn}-1)}$ to obtain new $\bar{\boldsymbol{P}}_e^{(I_{inn})}$;
5: **until** $\left|\mathrm{Tr}\big(\bar{\boldsymbol{P}}_e^{(I_{inn})}\big)-\lambda_{\max}\big(\bar{\boldsymbol{P}}_e^{(I_{inn})}\big)\right|\le\varepsilon_1$, where ε_1 is a sufficiently small positive scalar;
6: Perform eigenvalue decomposition and matrix reshape operation on $\bar{\boldsymbol{P}}_e^{(I_{inn})}$ to obtain $\widehat{\boldsymbol{P}}_e^{\star}$;

Output: Optimal PSFDA spatial pointing matrix $\widehat{\boldsymbol{P}}_e^{\star}$ for given $\boldsymbol{w}_{Tx}$ and $\boldsymbol{w}_{Rx}$.

problem (85) is an SDP problem with the linear objective function and convex constraints, which can be efficiently solved by the interior point method. Note that in the iterative optimization procedure for solving the problem (85), the initial $\bar{\boldsymbol{P}}_e^{(0)}$ is derived by solving the optimization problem (83) without considering its rank-1 constraint. Specifically, as demonstrated in [32], the value of the function $\mathrm{Tr}\big(\bar{\boldsymbol{P}}_e^{(t)}\big)-\lambda_{\max}\big(\bar{\boldsymbol{P}}_e^{(t)}\big)$ is monotonically decreasing as the iteration index t of the penalty function method increases, and converges to zero. In other words, by solving the iterative optimization problem (85), we can obtain a sequence of semi-positive definite matrices $\bar{\boldsymbol{P}}_e^{(t)}$, $t=1,2,\ldots,I_{\max}$, whose rank approaches 1, where $I_{\max}$ denotes the maximum iteration number. The corresponding locally optimal PSFDA spatial pointing matrix $\widehat{\boldsymbol{P}}_e^{\star}$ for the given $\boldsymbol{w}_{Tx}$ and $\boldsymbol{w}_{Rx}$ is calculated from $\bar{\boldsymbol{P}}_e^{(I_{\max})}$. Algorithm 1 summarizes the proposed iterative procedure for obtaining $\widehat{\boldsymbol{P}}_e^{\star}$.

D. Alternating Optimization Algorithm

By combining the solutions (62) and (69) as well as the optimization (83) minus its rank-1 constraint and the problem (85), the proposed alternating optimization algorithm alternatively optimizes $\big\{\boldsymbol{w}_{Tx},\boldsymbol{w}_{Rx},\boldsymbol{P}_e\big\}$, as summarized in Algorithm 2.

1) Convergence analysis: Consider arbitrary feasible $\boldsymbol{w}_{Rx}^{(I_{out})}$, $\boldsymbol{w}_{Tx}^{(I_{out})}$ and $\boldsymbol{P}_e^{(I_{out})}$ obtained at the I_{out}-th iteration of Algorithm 2. i) Given $\boldsymbol{w}_{Rx}^{(I_{out})}$ and $\boldsymbol{P}_e^{(I_{out})}$, the original SINR maximization problem (32) becomes a concave one, and the uniquely optimal $\boldsymbol{w}_{Tx}^{(I_{out}+1)}$ is obtained in (62). Therefore, after the step 2, we have $\mathrm{SINR}\big(\boldsymbol{w}_{Tx}^{(I_{out})},\boldsymbol{w}_{Rx}^{(I_{out})},\boldsymbol{P}_e^{(I_{out})}\big)\le\mathrm{SINR}\big(\boldsymbol{w}_{Tx}^{(I_{out}+1)},\boldsymbol{w}_{Rx}^{(I_{out})},\boldsymbol{P}_e^{(I_{out})}\big)$. ii) Similarly, based on $\boldsymbol{w}_{Tx}^{(I_{out}+1)}$ and $\boldsymbol{P}_e^{(I_{out})}$, the uniquely optimal $\boldsymbol{w}_{Rx}^{(I_{out}+1)}$ for the concave problem (32) is obtained in (69), which implies that $\mathrm{SINR}\big(\boldsymbol{w}_{Tx}^{(I_{out}+1)},\boldsymbol{w}_{Rx}^{(I_{out})},\boldsymbol{P}_e^{(I_{out})}\big)\le\mathrm{SINR}\big(\boldsymbol{w}_{Tx}^{(I_{out}+1)},\boldsymbol{w}_{Rx}^{(I_{out}+1)},\boldsymbol{P}_e^{(I_{out})}\big)$ after the step 3. iii) Given $\boldsymbol{w}_{Rx}^{(I_{out}+1)}$ and $\boldsymbol{w}_{Tx}^{(I_{out}+1)}$, the penalty function method, i.e., the step 4 of Algorithm 2, is guaranteed to converge to a locally optimal rank-1 $\boldsymbol{P}_e^{(I_{out}+1)}$ [32], which also satisfies $\mathrm{SINR}\big(\boldsymbol{w}_{Tx}^{(I_{out}+1)},\boldsymbol{w}_{Rx}^{(I_{out}+1)},\boldsymbol{P}_e^{(I_{out})}\big)\le\mathrm{SINR}\big(\boldsymbol{w}_{Tx}^{(I_{out}+1)},\boldsymbol{w}_{Rx}^{(I_{out}+1)},\boldsymbol{P}_e^{(I_{out}+1)}\big)$.

Algorithm 2: Proposed Alternating Optimization Algorithm.

Initialize: Give initial $\boldsymbol{w}_{Rx}^{(0)}$ and $\boldsymbol{P}_e^{(0)}$; Set initial SINR to $\mathrm{SINR}^{(0)}=0$; Set iteration index $I_{out}=0$;

1: **repeat**
2: For given $\boldsymbol{w}_{Rx}^{(I_{out})}$ and $\boldsymbol{P}_e^{(I_{out})}$, calculate optimal FDA Tx beamforming $\boldsymbol{w}_{Tx}^{(I_{out}+1)}$ from (62);
3: For given $\boldsymbol{w}_{Tx}^{(I_{out}+1)}$ and $\boldsymbol{P}_e^{(I_{out})}$, calculate optimal PSFDA Rx beamforming $\boldsymbol{w}_{Rx}^{(I_{out}+1)}$ from (69);
4: For given $\boldsymbol{w}_{Tx}^{(I_{out}+1)}$ and $\boldsymbol{w}_{Rx}^{(I_{out}+1)}$, call Algorithm 1 to obtain locally optimal PSFDA spatial pointing matrix $\boldsymbol{P}_e^{(I_{out}+1)}$;
5: Calculate achievable $\mathrm{SINR}^{(I_{out}+1)}$, which is the objective function of problem (32), using $\boldsymbol{w}_{Tx}^{(I_{out}+1)}$, $\boldsymbol{w}_{Rx}^{(I_{out}+1)}$ and $\boldsymbol{P}_e^{(I_{out}+1)}$;
6: $I_{out}=I_{out}+1$;
7: **until** $\left|\mathrm{SINR}^{(I_{out})}-\mathrm{SINR}^{(I_{out}-1)}\right|\le\epsilon$, where ϵ is a sufficiently small positive scalar;

Output: Suboptimal FDA Tx beamforming $\widetilde{\boldsymbol{w}}_{Tx}^{\star}=\boldsymbol{w}_{Tx}^{(I_{out})}$, PSFDA Rx beamforming $\widetilde{\boldsymbol{w}}_{Rx}^{\star}=\boldsymbol{w}_{Rx}^{(I_{out})}$ and PSFDA spatial pointing matrix $\widetilde{\boldsymbol{P}}_e^{\star}=\boldsymbol{P}_e^{(I_{out})}$; Corresponding maximum achievable SINR.

Combining i) to iii) leads to $\mathrm{SINR}\big(\boldsymbol{w}_{Tx}^{(I_{out})},\boldsymbol{w}_{Rx}^{(I_{out})},\boldsymbol{P}_e^{(I_{out})}\big)\le\mathrm{SINR}\big(\boldsymbol{w}_{Tx}^{(I_{out}+1)},\boldsymbol{w}_{Rx}^{(I_{out}+1)},\boldsymbol{P}_e^{(I_{out}+1)}\big)$. Thus the objective value of the SINR maximization (32) is monotonically increasing within each iteration of Algorithm 2. In addition, the set of the feasible solutions of the problem (32) is finite and closed, and the SINR is generally upper bounded by neglecting the noise term. Therefore, we conclude that the proposed alternating optimization algorithm is guaranteed to converge to a stationary SINR for the proposed polarization-subarray based FDA radar.

2) Complexity analysis: Since the steps 2 and 3 of Algorithm 2 involve the calculation of the semi-closed form optimal $\widehat{\boldsymbol{w}}_{Tx}^{\star}$ and $\widehat{\boldsymbol{w}}_{Rx}^{\star}$, the associated computational complexity is negligible. Thus, the computational complexity of the proposed alternating optimization mainly comes from the step 4 of optimizing $\boldsymbol{P}_e$ via the penalty function method. In the penalty function method, the SDP problem (85) needs to be solved iteratively. Clearly, the dimension of the positive semidefinite matrix in the problem (85) is $6N\times 6N$ and the number of constraints is $2N$. According to [35], the computational complexity for solving the SDP problem (85) with the interior point method is on the order of $\mathsf{O}\big(N^{4.5}\log\big(\frac{1}{\epsilon}\big)\big)$, for the given solution accuracy ϵ. Further define the maximum convergence numbers of iterations for Algorithm 1 and Algorithm 2 as $I_{inn}^{\max}$ and $I_{out}^{\max}$, respectively. The complexity of the proposed alternating optimization is on the order of $I_{out}^{\max}I_{inn}^{\max}\mathsf{O}\big(N^{4.5}\log\big(\frac{1}{\epsilon}\big)\big)$. In the simulation results of Section IV, we observe that the actual complexity is much lower than this worst-case bound.

E. Adaptive Joint Tx-Rx Beampattern Design

As described previously, with the knowledge of the interference sources' locations $\big(\theta_k,R_k\big)$, polarizations $\big(\alpha_k,\beta_k\big)$ and power σ_k^2 for $1\le k\le K$, the joint Tx-Rx beampattern can be

designed for the polarization-subarray based FDA radar based on the proposed alternating optimization algorithm. We first briefly discuss the adaptive realization of our proposed joint Tx-Rx beampattern design, namely, how to adaptively acquire $\big(\theta_k, R_k\big)$, $\big(\alpha_k, \beta_k\big)$ and σ_k^2 for $1 \leq k \leq K$. Then we discuss how to utilize the acquired interference information for target localization. Actually, the adaptive radar beampattern design for target search has been introduced in [27]–[29], in which the Tx waveform covariance matrices are designed based on the interference information from previous observations.

Similarly to [27], [28], we can send the selected training waveforms, $\boldsymbol{s}_{Tx}(l)$ for $l = 1, \ldots, N_{\text{training}}$, to explore the environment when the target is absent. The estimates of $\big(\theta_k, R_k\big)$, $\big(\alpha_k, \beta_k\big)$ and σ_k^2 can then be adaptively acquired from the received training signals by jointly utilizing the rank-reduced polarization ESPRIT and MUSIC algorithms [34] as well as the least squares estimation [27].

Then similarly to [28], we consider an iterative process between Algorithm 2 for adaptively deriving the optimal $\big\{\boldsymbol{w}_{Tx}, \boldsymbol{w}_{Rx}, \boldsymbol{P}_e\big\}$ based on these estimates and the spatial-polarized spectrum peak search for target localization. To be specific, the spatial-polarized spectrum search for target localization is defined as

$$\big(\widehat{R}_0, \widehat{\boldsymbol{\delta}}_0\big) = \arg\max_{(R,\boldsymbol{\delta})} \frac{\boldsymbol{w}_{Rx}^{\mathrm{H}}(R,\boldsymbol{\delta})\big(\boldsymbol{R}_{YY} - \widehat{\boldsymbol{R}}_{IN}\big)\boldsymbol{w}_{Rx}(R,\boldsymbol{\delta})}{\boldsymbol{w}_{Rx}^{\mathrm{H}}(R,\boldsymbol{\delta})\widehat{\boldsymbol{R}}_{IN}\boldsymbol{w}_{Rx}(R,\boldsymbol{\delta})}, \tag{86}$$

where $\boldsymbol{w}_{Rx}(R,\boldsymbol{\delta})$ is derived from Algorithm 2 and $\boldsymbol{R}_{YY}$ denotes the sample covariance matrix of the received signal at PSFDA, while the interferences plus noise covariance matrix $\widehat{\boldsymbol{R}}_{IN}$ is based on the pre-estimated interferences information. The detailed iterative process for this spatial-polarized spectrum search for target localization can be found in [28].

F. Application to Multitarget Scenario

Our proposed polarization-subarray based FDA radar can also be applied to the multitarget scenario in the existence of multiple interferences. However, the output SINR maximization based joint Tx-Rx beampattern design presented in this work is unsuitable for multitarget localization. Referring to [12], [13], [17], [28], we can utilize the polarization-subarray based FDA MIMO radar to increase the design freedom of the Tx beampattern. Since the interference plus noise can be viewed as a spatially colored noise, it is intuitive to mitigate the interference via the widely adopted colored-noise prewhitening process [17]. Specifically, based on the eigenvalue decomposition of $\widehat{\boldsymbol{R}}_{IN} = \widehat{\boldsymbol{U}}_{IN}\boldsymbol{\Lambda}_{IN}\widehat{\boldsymbol{U}}_{IN}^{\mathrm{H}}$, a preprocessing matrix $\widehat{\boldsymbol{T}}_{IN} = \boldsymbol{\Lambda}_{IN}^{-\frac{1}{2}}\widehat{\boldsymbol{U}}_{IN}^{\mathrm{H}}$ is obtained and it is then applied to the received signal in (17) to similarly obtain the interference-whitened received signal at the PSFDA. Similar to the single target case, the interferences' information can be estimated by collecting the training data in the absence of targets.

The main challenging for multitarget localization is the effective Tx beampattern design. In the existing literature, one popular solution is to design the Tx beamforming matrix for realizing the desired Tx beampattern while suppressing the sidelobe interferences as much as possible. Generally, the desired Tx beampattern is preset for the known target. However, when the knowledge of the target location is unavailable, this desired Tx beampattern is difficult to obtain. In this context, we can extend the iterative joint Tx-Rx beampattern design for multitarget localization proposed in [28] to our polarization-subarray based FDA MIMO radar. This topic is however beyond the scope of our current work.

IV. Simulation Study and Result Discussions

Unless otherwise stated, the two-subarray based UL Tx FDA consists of $2N = 20$ antennas, which are deployed within half a wavelength distance from each other, i.e., $d = \frac{c_0}{2f_0}$. The carrier frequency is set as $f_0 = 15$ GHz. The same antenna array setting is also applied to the UL Rx PSFDA, and the PSFDA's polarization gain is given by $G_e = 1$. This polarization-subarray based UL FDA radar is denoted by FDA-PSFDA for short. The Tx plus duration is set to $T_p = 0.2$ ms and the output SINR maximization is considered at $t = t_0 = 0.2$ ms. The interested far field target location is $(\theta_0, R_0) = \big(45^\circ, 100\,\text{km}\big)$ and the desired target signal's polarization is $\big(\alpha_0, \beta_0\big) = \big(60^\circ, 0^\circ\big)$. There also exists one interference source located at (θ_1, R_1), and the polarization of the interfering signal is $(\alpha_1, \beta_1) = \big(\alpha_1, 0^\circ\big)$. The actual azimuth angles of the target and interference sources are assumed to be $\phi_0 = \phi_1 = 90^\circ$. The desired signal signal to noise ratio (SNR) is defined as $10\log_{10}\frac{\sigma_0^2}{\sigma_\xi^2}$. The target signal power and the interference power are $\sigma_0^2 = 5$ dB and $\sigma_1^2 = 15$ dB, respectively, while the unit noise power is $\sigma_\xi^2 = 1$. The spatial range, angle and polarization distance between the desired target signal and the interfering signal, denoted as Δ_r, Δ_a and Δ_p, are defined respectively by

$$\Delta_r = |R_1 - 100\,\text{km}|, \tag{87}$$

$$\Delta_a = |\theta_1 - 45^\circ|, \tag{88}$$

$$\Delta_p = \arccos\Big(\cos 2\beta_0 \cos 2\beta_1 \cos\big(2(\alpha_0 - \alpha_1)\big) + \sin 2\beta_0 \sin 2\beta_1\Big) = 2|60^\circ - \alpha_1|. \tag{89}$$

The CVX toolbox is utilized to solve the standard convex SDP problem (85). The basic FDA radar, the conventional PA radar and the LFO-FDA radar are adopted as three comparisons in order to demonstrate the superior performance of the proposed FDA-PSFDA radar. All the three benchmark radars have 20 Tx antennas and 20 Rx antennas.

As shown in Section II-D, our work for the polarization-subarray based UL FDA radar can be extended to the polarization-subarray based URP FDA radar, denoted as URP FDA-PSFDA. Thus we also consider the URP FDA-PSFDA radar, whose Tx URP FDA consists of two UL subarray-based Tx FDAs with a total of $4N = 40$ antenna elements. This same deployment is also applied to the Rx URP PSFDA.

A. Proposed Joint Time-Invariant Tx-Rx Beampattern

To investigate the proposed joint Tx-Rx beampattern design for the FDA-PSFDA radar, we use the normalized joint Tx-Rx beampattern as the performance metric, which is defined by

$$\bar{B}(t_0; R, \boldsymbol{\delta}) = \frac{\Big|\boldsymbol{w}_R^{\star\mathrm{H}}\big(\boldsymbol{a}_J(t_0; R, \boldsymbol{\delta}) \odot \big(\boldsymbol{1}_{2N} \otimes \boldsymbol{w}_{Tx}^\star\big)\big)\Big|^2}{\Big|\boldsymbol{w}_{Rx}^{\star\mathrm{H}}\big(\boldsymbol{a}_J(t_0; R_0, \boldsymbol{\delta}_0) \odot \big(\boldsymbol{1}_{2N} \otimes \boldsymbol{w}_{Tx}^\star\big)\big)\Big|^2}, \tag{90}$$

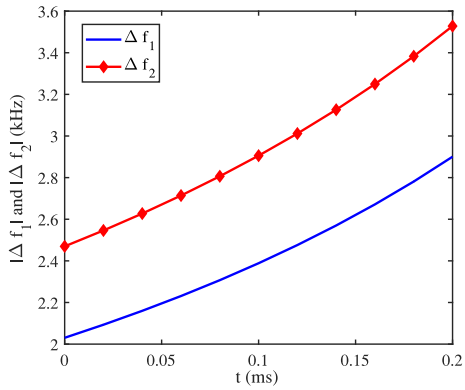

Fig. 4. The time-dependent frequency offsets designed for the proposed FDA-PSFDA radar.

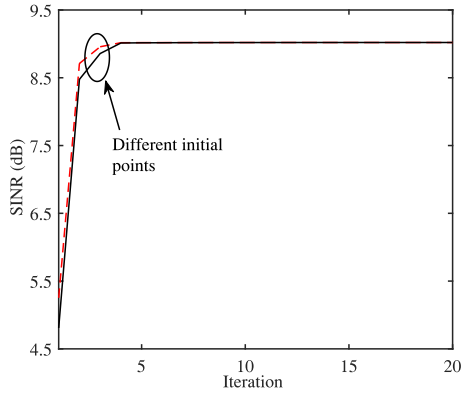

Fig. 5. The convergence of the proposed alternating optimization algorithm.

where the locally optimal $\boldsymbol{w}_{Tx}^{\star}$, $\boldsymbol{w}_{Rx}^{\star}$ and $\boldsymbol{P}_e^{\star}$ are obtained by Algorithm 2. In this investigation, the interference source is located at $(50^\circ, 99.5\,\text{km})$ and its polarization is $\left(40^\circ, 0^\circ\right)$.

For the sake of achieving the time-invariant joint Tx-Rx beampattern at the target, the time-dependent frequency offsets Δf_1 and Δf_2 of the proposed FDA-PSFDA radar are first designed according to (28), and they are shown in Fig. 4. As expected, the values of $\Delta f_1(t)$ and $\Delta f_2(t)$ are remarkably small, in comparison to the carrier frequency $f_0 = 15$ GHz. Based on the obtained $\Delta f_1(t)$ and $\Delta f_2(t)$, Fig. 5 depicts the convergence performance of the proposed alternating optimization algorithm, Algorithm 2, in terms of the achievable SINR (31) versus the number of iterations. It can be seen that Algorithm 2 converges within 5 iterations for the two given different initial points $\{\boldsymbol{w}_{Rx}^{(0)}, \boldsymbol{P}_e^{(0)}\}$.

In Fig. 6, we investigate the normalized joint Tx-Rx beampattern (90) of the proposed FDA-PSFDA radar in the range-time (R, t) dimensions at two different spatial angles. Specifically, in Fig. 6(a), we fix the spatial angle to that of the target, namely, $\theta = \theta_0 = 45^\circ$. It can be seen from Fig. 6(a) that the maximum beampattern is achieved at the target range $R = R_0 = 100$ km and it is also time invariant. This confirms the effectiveness of our proposed beampattern design, that is, the beampattern is maximized at the target location and it is time invariant over the whole pulse duration. By contrast, when the spatial angle is fixed to that of the interference, i.e., $\theta = \theta_1 = 50^\circ$, in Fig. 6(b), it is clear that the beam gain at the interference location

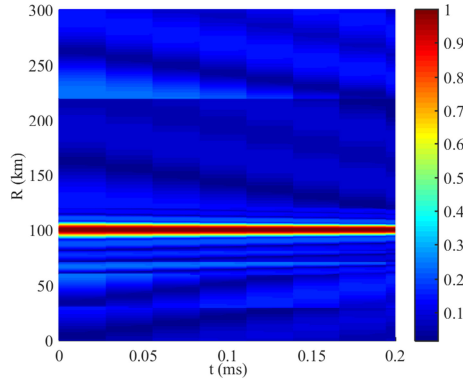

(a) Fixed angle $\theta = 45^\circ$

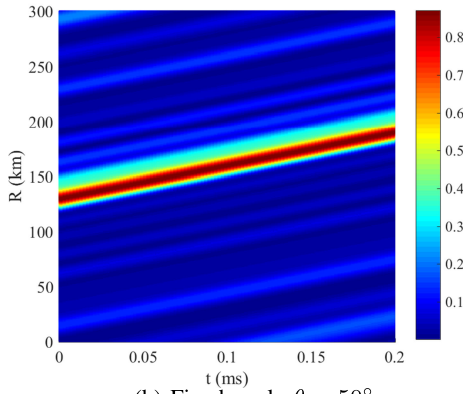

(b) Fixed angle $\theta = 50^\circ$

Fig. 6. Range-time beampattern $\bar{B}(t_0; R, \boldsymbol{\delta})$ of the FDA-PSFDA radar.

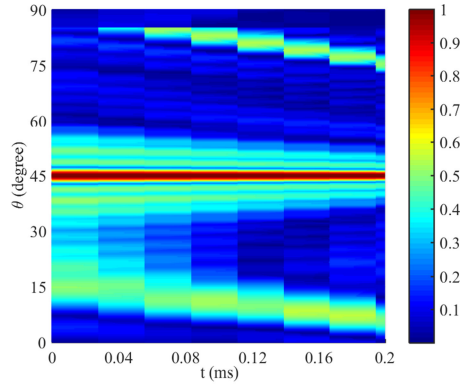

(a) Fixed range $R = 100\,\text{km}$

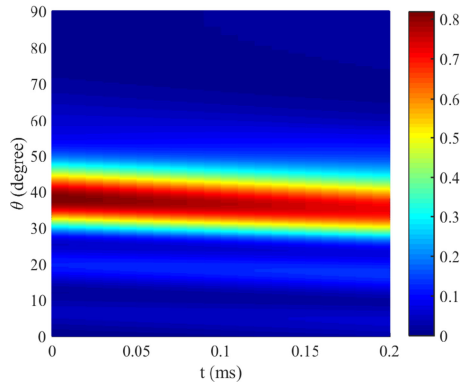

(b) Fixed range $R = 99.5\,\text{km}$

Fig. 7. Angle-time beampattern $\bar{B}(t; R, \boldsymbol{\delta})$ of the FDA-PSFDA radar.

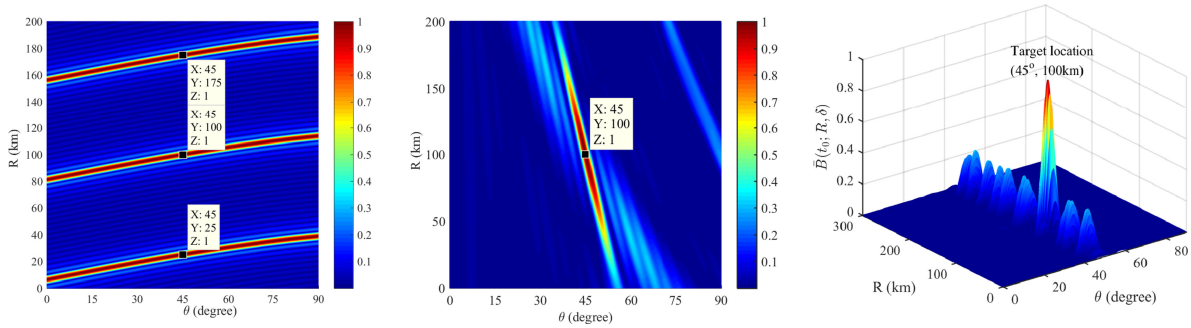

(a) Basic FDA (b) FDA-PSFDA (c) URP FDA-PSFDA

Fig. 8. Beampattern $\bar{B}(t_0; R, \boldsymbol{\delta})$ comparison of basic FDA radar, FDA-PSFDA radar and URP FDA-PSFDA radar at time $t_0 = 0.2$ ms.

$(50^\circ, 99.5\,\text{km})$ is remarkably reduced over the whole duration. Moreover, in this case, the maximum value of the normalized beampattern is about 0.85 and the corresponding location is time-varying.

Fig. 7 depicts the normalized joint Tx-Rx beampattern (90) of the proposed FDA-PSFDA radar in the angle-time (θ, t) dimensions at two different spatial distances. For the case of the fixed $R = R_0 = 100$ km shown in Fig. 7(a), the maximum beampattern only occurs at the target angle $\theta = \theta_0 = 45^\circ$ and it is time-invariant over the whole pulse duration. By contrast, for the case of $R = R_1 = 99.5$ km shown in Fig. 7(b), the location of the maximum beampattern is not kept at the target angle $\theta = \theta_0 = 45^\circ$ and it drifts with time.

Furthermore, Fig. 8(a) depicts the normalized joint Tx-Rx beampattern (90) in the range-angle (R, θ) dimensions at the time $t_0 = 0.2$ ms, for the basic FDA radar, in comparison with the normalized joint Tx-Rx beampattern of the FDA-PSFDA radar shown in Fig. 8(b). For the basic FDA radar, the carrier frequency is $f_0 = 15$ GHz and the frequency offset is $\Delta f = 4$ kHz. Naturally, Fig. 8(b) confirms that the proposed FDA-PSFDA radar achieves the single-maximum joint Tx-Rx beampattern at the target location, while the joint Tx-Rx beampattern of the basic FDA radar depicted in Fig. 8(a) has multiple maximum locations due to the range periodicity of $\Delta R = \frac{c_0}{\Delta f} = 75$ km. To demonstrate that the single-maximum joint Tx-Rx beampattern of the URP FDA-PSFDA can also be achieved by the proposed alternating optimization, Fig. 8(c) plots the three-dimensional joint Tx-Rx beampattern $\bar{B}(t_0; R, \boldsymbol{\delta})$ for the URP FDA-PSFDA radar.

Note that the LFO-FDA radar proposed in [20] also achieves the range-angle decoupled beampattern at the target location. Therefore, in Fig. 9, we also compare the joint Tx-Rx beampattern of the LFO-FDA radar with those of the basic FDA and FDA-PSFDA radars in the range-angle domain $(R, 45^\circ)$ at two different times $t_0 = 0.1$ ms and $t_0 = 0.2$ ms. The results of Fig. 9 confirm that the joint Tx-Rx beampatterns of both the LFO-FDA radar and the basic FDA radar are time-varying, while our FDA-PSFDA radar achieves the time-invariant focusing beampattern at the target direction $(45^\circ, 100\,\text{km})$. Hence, we infer that unlike the basic FDA and LFO-FDA radars, the proposed FDA-PSFDA radar is capable of realizing the accurate target localization consistently.

B. Output SINR Comparison

To demonstrate the advantages of the proposed FDA-PSFDA radar, Fig. 10 compares the output SINR performance of the

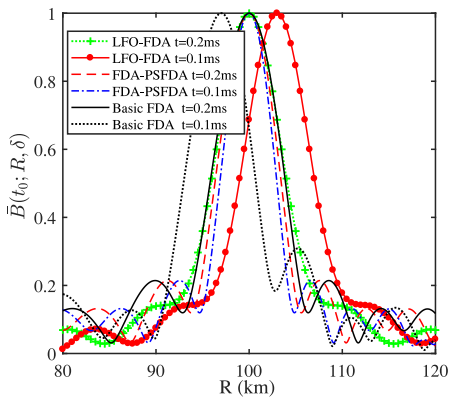

Fig. 9. Comparison of the beampatterns $\bar{B}(t_0; R, \boldsymbol{\delta})$ in the range-angle domain $(R, 45^\circ)$ at $t_0 = 0.1$ ms and $t_0 = 0.2$ ms for the basic FDA, LFO-FDA and FDA-PSFDA radars.

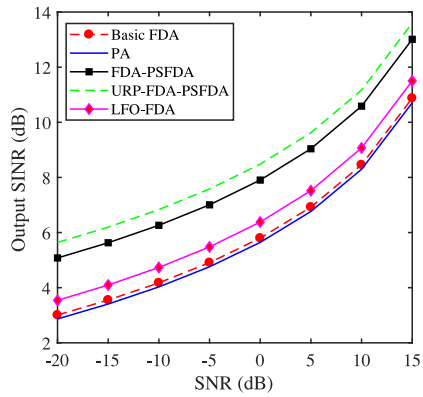

Fig. 10. The SINR performance of five radars as the functions of SNR at the fixed time $t_0 = 0.2$ ms.

five radars as the functions of SNR. Here, we consider the interference location $(50^\circ, 99.5\,\text{km})$ with the polarization $(40^\circ, 0^\circ)$, which is spatially close to the target, and the polarization distance (89) is $\Delta_p = 20^\circ$. From Fig. 10, it is seen that the PA radar attains the lowest SINR, and the basic FDA radar is slightly better. Compared to the basic FDA radar with a constant frequency offset, by introducing the nonlinear frequency offsets among array elements, the LFO-FDA radar increases the design freedom of beampattern and thus realizes a higher SINR. More importantly, the proposed FDA-PSFDA radar significantly outperforms the other two FDA radars, because it is capable of

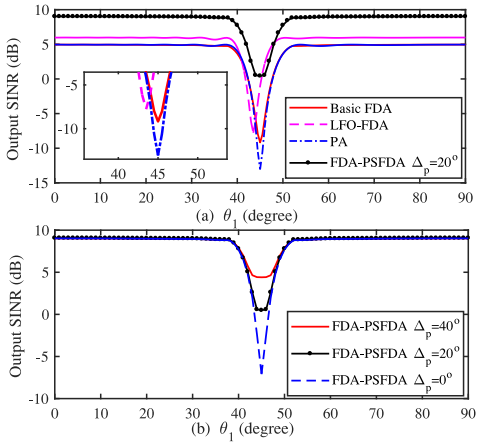

Fig. 11. The SINR performance as the functions of the interference DOA θ_1 at time $t_0 = 0.2$ ms and given the range distance $\Delta_r = 100$ m: (a) four radars with $\Delta_p = 20^\circ$, and (b) FDA-PSFDA radar with different Δ_p.

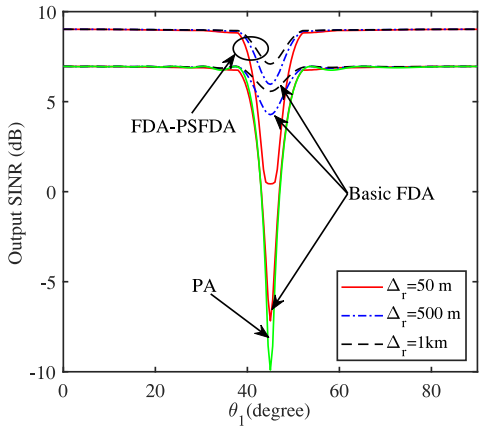

Fig. 12. The SINR performance of the three radars as the functions of the interference signal DOA θ_1 at time $t_0 = 0.2$ ms, given different range distances Δ_r and the polarization distance $\Delta_p = 20^\circ$.

utilizing the polarization distance $\Delta_p = 20^\circ$ to separate the spatially close signals. Because for this example the azimuth angles of the target and interference are both $\phi_0 = \phi_1 = 90^\circ$, the better performance of the URP FDA-PSFDA radar over the (UL) FDA-PSFDA radar is mainly due to it having more antenna elements at both transmitter and receiver. For other azimuth angle values, the URP FDA-PSFDA radar can utilize the extra degree of freedom in the azimuth domain to further enhance the performance.

Next, Fig. 11(a) compares the output SINR performance of the four radars as the functions of the interference signal DOA θ_1 at time $t_0 = 0.2$ ms, where the range distance $\Delta_r = 100$ m and the polarization distance $\Delta_p = 20^\circ$ are adopted. Note that the PA, basic FDA and LFO-FDA radars cannot exploit the signal's polarization information. Observe from Fig. 11(a) that when the angle distance (88) $\Delta_a \leq 5^\circ$, the output SINR performance deteriorates due to the fact that the target and interference are spatially close. In particular, at $\Delta_a = 0^\circ$, i.e., the target and interference are spatially indistinguishable, the SINR of the PA radar is below -12 dB, since the PA radar only has the angle-dependent beampattern, while the SINRs of the basic FDA radar and the LFO-FDA radar are approximately -8 dB and -4 dB, respectively. This is because the LFO-FDA radar has more flexible frequency offsets than the basic FDA radar, and it can utilize the small range distance $\Delta_r = 100$ m to realize a higher SINR. The output SINR of our FDA-PSFDA radar is about 4 dB higher than the LFO-FDA radar, because it is capable of utilizing the polarization distance $\Delta_p = 20^\circ$ to enhance the performance. In addition, we also observe that when the target and the interference are spatially well separated, i.e., $\Delta_a > 10^\circ$, the performance of all the four radars are approximately independent of θ_1. In this case, the FDA-PSFDA radar attains about 3 dB of the SINR gain over the second best LFO-FDA radar. The above observations confirm the advantage of the FDA-PSFDA radar in suppressing interference via the array polarization optimization, especially when the target and interference are spatially close.

Furthermore, Fig. 11(b) compares the achievable output SINR performance of the FDA-PSFDA radar given three different polarization differences Δ_p. Observe that with the small range distance $\Delta_r = 100$ m and at the angle distance $\Delta_a = 0^\circ$, i.e., the target and interference are spatially indistinguishable, the output SINR performance of the FDA-PSFDA radar are -7 dB, 0 dB and 5 dB, respectively, given the polarization differences $\Delta_p = 0^\circ$, 20° and 40°. This again indicates that for the spatially indistinguishable target and interference, the proposed FDA-PSFDA radar can effectively utilize the polarization distance to enhance the output SINR.

To further demonstrate the range-dependent interference suppression capability of the FDA-PSFDA radar, we adopt the PA and basic FDA radars as comparisons in Fig. 12. Specifically, Fig. 12 depicts the output SINR performance of these three radars as the functions of the interference DOA θ_1 at $t_0 = 0.2$ ms, for different spatial range differences Δ_r and given the polarization difference $\Delta_p = 20^\circ$. Note that the output SINR of the PA radar is not influenced by the range difference Δ_r owing to its angle-dependent beampattern. Therefore, only the single SINR curve of the PA radar for $\Delta_r = 50$ m is shown in Fig. 12. Observe that at $\Delta_a = 0^\circ$, increasing Δ_r improves the output SINRs of the basic FDA radar and the FDA-PSFDA radar. The results of Fig. 12 also confirm the superior SINR performance of the FDA-PSFDA radar over the basic FDA radar.

C. Target Range and Angle Estimation

We now study the target localization performance of the FDA-PSFDA radar. As in [27], [28], we assume that the interference source location $(50^\circ, 99.5\,\text{km})$ and its polarization $(40^\circ, 0^\circ)$ are pre-estimated with high SNR. The target and interference powers are again fixed to $\sigma_0^2 = 5$ dB and $\sigma_1^2 = 15$ dB. As presented in Section III-E, to realize the accurate target localization, we can employ the iterative process between Algorithm 2 for deriving the locally optimal $\{\boldsymbol{w}_{Tx}, \boldsymbol{w}_{Rx}, \boldsymbol{P}_e\}$ and the spatial-polarized spectral peak search based on (86). Since the basic FDA radar has the coupling range-angle beam response, we adopt the PA and LFO-FDA radars as two comparisons. All the estimates are obtained based on 1024 samples and 200 Monte Carlo runs.

In Fig. 13, the root mean square errors (RMSEs) of the angle and range estimates as the functions of SNR are shown. From Fig. 13(a), it is clear that the angle estimation accuracy of the proposed FDA-PSFDA radar is close to that of the PA radar and it is marginally better than that of the LFO-FDA radar. However, since the range of the target cannot be estimated by the PA radar, Fig. 13(b) only shows the RMSEs of the range estimation for the LFO-FDA and FDA-PSFDA radars. From Fig. 13(b) we

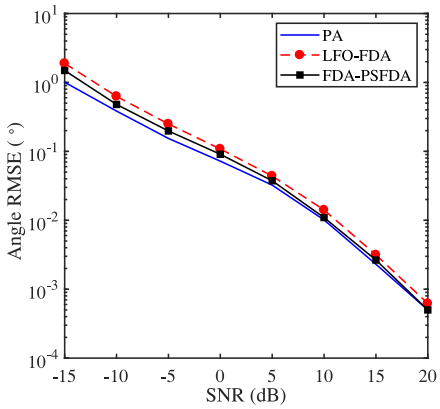

(a) Angle estimation

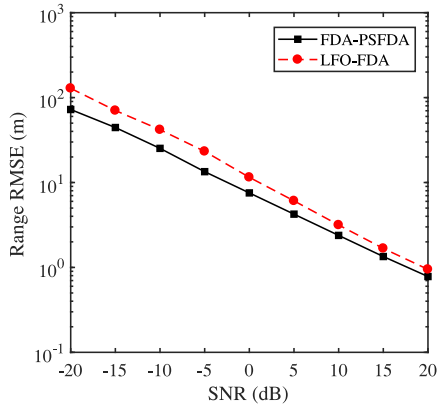

(b) Range estimation

Fig. 13. Angle and range RMSE performance as the functions of SNR for the three radars at time $t_0 = 0.2$ ms and polarization distance $\Delta_p = 20°$.

clearly see that the FDA-PSFDA radar outperforms the LFO-FDA radar in the range estimation. In summary, by introducing the extra design freedom in polarization domain for distinguishing the spatially closed signals, the proposed FDA-PSFDA radar achieves better target localization performance than the LFO-FDA radar.

V. Conclusions

In this paper, we have proposed a novel polarization-subarray based FDA radar with the subarray-based UL FDA as transmit array and the polarization-sensitive subarray-based UL FDA as the receive array. This novel structure exploits the subarray-based FDA to achieve a single-maximum beampattern at the desired target location, while utilizing the polarization sensitivity of the PSFDA to improve the output SINR. To realize the accurate target localization, the time-invariant joint Tx-Rx beampattern at the target location has been considered via the time-dependent frequency offsets design, and the optimal joint Tx-Rx beampattern of the proposed polarization-subarray based FDA radar has been derived based on the output SINR maximization. To effectively solve this nonconvex SINR maximization problem, a suboptimal alternating optimization algorithm has been derived to optimize the FDA Tx beamforming, the PSFDA Rx beamforming and the PSFDA spatial pointing matrix iteratively. Numerical simulation results have demonstrated that the time-invariant and single maximum joint Tx-Rx beampattern at the target location over the whole pulse duration is achieved by the proposed polarization-subarray based FDA radar based on the alternating optimization algorithm. Our results have confirmed that the achievable output SINR performance of the polarization-subarray-based FDA radar is significantly higher than those of the PA radar and the existing FDA radars, especially when the target and interference are spatially indistinguishable. We have also shown that our approach can readily be extended to the polarization-subarray based URP FDA radar.

References

[1] K. Gao, W. Q. Wang, H. Chen, and J. Cai, "Transmit beamspace design for multi-carrier frequency diverse array sensor," *IEEE Sensors J.*, vol. 16, no. 14, pp. 5709–5714, Jul. 2016.

[2] M. C. Wicks and P. Antonik, "Frequency diverse array with independent modulation of frequency, amplitude, and phase," U.S. Patent, 7 319 427, Jan. 2008.

[3] P. Antonik, M. C. Wicks, H. D. Griffiths, and C. J. Baker, "Frequency diverse array radars," in *Proc. IEEE Radar Conf.*, Verona, NY, Apr. 2006, pp. 215–217.

[4] Z. Li *et al.*, "Reducing mutual coupling of MIMO antennas with parasitic elements for mobile terminals," *IEEE Trans. Antennas Propag.*, vol. 60, no. 2, pp. 473–481, Feb. 2012.

[5] S. M. Lin, "Characteristics of frequency scanning array," in *Proc. Antennas Propag. Soc. Int. Symp.*, Vancouver, Canada, Jun. 17-21, 1985, pp. 131–134.

[6] D. Zhao and Y. Wei, "Adaptive gradient search for optimal sidelobe design of hopped-frequency waveform," *IET Radar, Sonar Navigation*, vol. 8, no. 4, pp. 282–289, Apr. 2014.

[7] M. Secmen, S. Demir, A. Hizal, and T. Eker, "Frequency diverse array antenna with periodic time modulated pattern in range and angle," in *Proc. IEEE Radar Conf.*, Apr. 2007, pp. 427–430.

[8] W. Q. Wang, "Frequency diverse array antenna: New opportunities," *IEEE Antennas Propag. Mag.*, vol. 57, no. 2, pp. 145–152, Apr. 2015.

[9] P. Baizert, T. B. Hale, M. A. Temple, and M. C. Wicks, "Forward-looking radar GMIT benefits using a linear frequency diverse array," *Electron. Lett.*, vol. 42, no. 22, pp. 1311–1312, Oct. 2006.

[10] C. Cetintepe and S. Demir, "Multipath characteristics of frequency diverse arrays over a ground plane," *IEEE Trans. Antennas Propag.*, vol. 62, no. 7, pp. 3567–3574, Jul. 2014.

[11] W. Q. Wang, "Range-angle dependent transmit beampattern synthesis for linear frequency diverse arrays," *IEEE Trans. Antennas Propag.*, vol. 61, no. 8, pp. 4073–4081, Aug. 2013.

[12] J. Xu, G. Lia, S. Zhu, and H. C. So, "Deceptive jamming suppression with frequency diverse MIMO radar," *Signal Process.*, vol. 113, pp. 9–17, Aug. 2015.

[13] J. Xu *et al.*, "An adaptive range-angle-Doppler processing approach for FDA-MIMO radar using three-dimensional localization," *IEEE J. Sel. Topics Signal Process.*, vol. 11, no. 2, pp. 309–320, Mar. 2017.

[14] W. Khan, I. M. Qureshi, A. Basit, and B. Shoaib, "Transmit/received beamforming for MIMO log-frequency diverse array radar," in *Proc. Int. Bhurban Conf. Appl. Sci. Technol.*, Islamabad, Pakistan, Jan. 12–16, 2016, pp. 689–693.

[15] Y. Liu, H. Ruan, L. Wang, and A. Nehorai, "The random frequency diverse array: A new antenna structure for uncoupled direction-range indication in active sensing," *IEEE J. Sel. Topics Signal Process.*, vol. 11, no. 2, pp. 295–308, Mar. 2017.

[16] W. Q. Wang, "Subarray-based frequency diverse array radar for target range-angle estimation," *IEEE Trans. Aerosp. Electron. Syst.*, vol. 50, no. 4, pp. 3057–3067, Oct. 2014.

[17] W. Q. Wang and H. C. So, "Transmit subaperturing for range and angle estimation in frequency diverse array radar," *IEEE Trans. Signal Process.*, vol. 62, no. 8, pp. 2000–2011, Apr. 2014.

[18] W. Khan, I. M. Qureshi, A. Basit, and W. Khan, "Range-bins-based MIMO frequency diverse array radar with logarithmic frequency offset," *IEEE Antennas Wireless Propag. Lett.*, vol. 15, pp. 885–888, 2016.

[19] W. Khan and I. M. Qureshi, "Frequency diverse array radar with time-dependent frequency offset," *IEEE Antennas Wireless Propag. Lett.*, vol. 13, pp. 758–761, Apr. 2014.

[20] A. M. Yao, W. Wu, and D. G. Fang, "Frequency diverse array antenna using time-modulated optimized frequency offset to obtain time-invariant spatial fine focusing beampattern," *IEEE Trans. Antennas Propag.*, vol. 64, no. 10, pp. 4434–4446, Oct. 2016.
[21] A. Nehorai, K. C. Ho, and B. T. G. Tan, "Minimum-noise-variance beamformer with an electromagnetic vector sensor," *IEEE Trans. Signal Process.*, vol. 47, no. 3, pp. 601–618, Mar. 1999.
[22] R. M. Narayanan, K. Atanassov, V. Stoiljkovic, and G. R. Kadambi, "Polarization diversity measurements and analysis for antenna configurations at 1800 MHz," *IEEE Trans. Antennas Propag.*, vol. 52, no. 7, pp. 1795–1810, Jul. 2004.
[23] D. P. Stapor, "Optimal receive antenna polarization in the presence of interference and noise," *IEEE Trans. Antennas Propag.*, vol. 43, no. 5, pp. 473–477, May 1995.
[24] S. Gong, C. Xing, S. Chen, and Z. Fei, "Secure communications for dual-polarized MIMO radars," *IEEE Trans. Signal Process.*, vol. 65, no. 16, pp. 4177–4192, Aug. 2017.
[25] S. Gong, C. Xing, S. Chen, and Z. Fei, "Polarization sensitive array based physical-layer security," *IEEE Trans. Veh. Technol.*, vol. 67, no. 5, pp. 3964–3981, May 2018.
[26] H. Chen, H. Shao, and W. Wang, "Sparse reconstruction-based angle-range-polarization-dependent beamforming with polarization sensitive frequency diverse array," in *Proc. Int. Conf. Acoust., Speech, Signal Process.*, Shanghai, China, Mar. 20–25, 2016, pp. 2891–2895.
[27] Z. Chen, H. Li, G. Cui, and M. Rangaswamy, "Adaptive transmit and receive beamforming for interference mitigation," *IEEE Signal Process. Lett.*, vol. 21, no. 2, pp. 235–239, Feb. 2014.
[28] K. Luo and A. Manikas, "Joint transmitter-receiver optimization in multitarget MIMO radar," *IEEE Trans. Signal Process.*, vol. 65, no. 23, pp. 6292–6302, Dec. 2017.
[29] J. Liu, H. Li, and B. Himed, "Joint optimization of transmit and receive beamforming in active arrays," *IEEE Signal Process. Lett.*, vol. 21, no. 1, pp. 39–42, Jan. 2014.
[30] Y. Xu, X. Shi, J. Xu, and P. Li, "Range-angle-dependent beamforming of pulsed frequency diverse array," *IEEE Trans. Antennas Propag.*, vol. 63, no. 7, pp. 3262–3267, Jul. 2015.
[31] A. M. Jones and B. D. Rigling, "Frequency diverse array radar receiver architectures," in *Proc. Int. Waveform Diversity Des. Conf.*, Kauai, HI, Jan. 22–27, 2012, pp. 211–217.
[32] H. M. Wang, M. Luo, Q. Yin, and X. G. Xia, "Hybrid cooperative beamforming and jamming for physical-layer security of two-way relay networks," *IEEE Trans. Inf. Forensics Secur.*, vol. 8, no. 12, pp. 2007–2020, Dec. 2013.
[33] A. Charnes and W. W. Cooper, "Programming with linear fractional functionals," *Naval Res. Logistics*, vol. 9, nos. 3/4, pp. 181–186, 1962.
[34] W. Si, Y. Wang, C. Hou, and H. Wang, "Real-valued 2D MUSIC algorithm based on modified forward/backward averaging using an arbitrary centrosymmetric polarization sensitive array," *Sensors*, vol. 17, no. 10, pp. 1–16, 2017.
[35] A. Ben-Tal and A. Nemirovski, *Lectures on Modern Convex Optimization: Analysis, Algorithms, and Engineering Applications*. Philadelphia, PA, USA: SIAM, 2001.

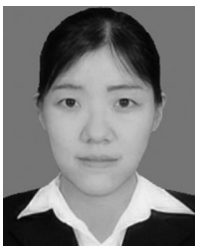

Shiqi Gong (S'15) received the B.S. degree in electronic engineering from Beijing Institute of Technology, Beijing, China, in 2014. She is working toward the Ph.D. degree in the School of Electronic and Information, Beijing Institute of Technology. Meanwhile, she is also a Research Assistant with the University of Macau, Macau, China. Her research interests include array signal processing, physical-layer security, resource allocation, and convex optimization.

Shuai Wang (M'18) received the B.Eng. and Ph.D. degrees from Zhengzhou University, Zhengzhou, China, and Beijing Institute of Technology, Beijing, China, in 2005 and 2012, respectively, both in the major of communications engineering, and both with the highest honor. He won the award for "outstanding Ph.D. dissertation" granted by the Beijing Municipal Education Commission in 2013 with other 49 co-winners, nominated from all the Ph.D. graduates that received their degrees in Beijing that year. From September 2010 to 2011, he was a visiting Ph.D. student in the School of Electronics and Computer Science, University of Southampton, U.K. Since July 2012, he has been with the School of Information Science and Electronics, Beijing Institute of Technology, where he is currently an Associate Professor. His research interest includes channel estimation, anti-jamming transmission, synchronization techniques, and beamforming. He has authored or coauthored more than 20 peer-reviewed articles, mainly in leading IEEE journals or conferences. He was or currently is the Principal Investigator for 12 research funds, including two granted by the National Science Foundation of China. He is a recipient of the (Second Class) Scientific and Technical Progress Award granted by the Ministry of Industry and Information Technology of China. He also holds 17 patents.

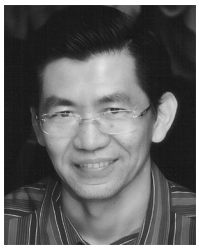

Sheng Chen (M'90–SM'97–F'08) received the B.Eng. degree from the East China Petroleum Institute, Dongying, China, in 1982, and the Ph.D. degree from the City University, London, U.K., in 1986, both in control engineering, and the higher doctoral degree, Doctor of Sciences (D.Sc.), from the University of Southampton, Southampton, U.K.

From 1986 to 1999, he held research and academic appointments at the Universities of Sheffield, Edinburgh, and Portsmouth, all in U.K. Since 1999, he has been with the Departmen of Electronics and Computer Science, University of Southampton, U.K., where he is currently a Professor of intelligent systems and signal processing. His research interests include adaptive signal processing, wireless communications, modeling and identification of nonlinear systems, neural network and machine learning, intelligent control system design, evolutionary computation methods, and optimization. He has authored or coauthored more than 550 research papers.

Dr. Chen is a Fellow of the United Kingdom Royal Academy of Engineering, a Fellow of IET, a Distinguished Adjunct Professor at King Abdulaziz University, Jeddah, Saudi Arabia, and an ISI highly cited researcher in engineering (Mar. 2004).

Chengwen Xing (S'08–M'10) received the B.Eng. degree from Xidian University, Xi'an, China, in 2005, and the Ph.D. degree from the University of Hong Kong, Hong Kong, China, in 2010. Since September 2010, he has been with the School of Information and Electronics, Beijing Institute of Technology, Beijing, China, where he is currently a Full Professor. From September 2012 to December 2012, he was a visiting scholar at the University of Macau. His current research interests include statistical signal processing, convex optimization, multivariate statistics, combinatorial optimization, massive MIMO systems, and high frequency band communication systems. He is an Associate Editor for the IEEE TRANSACTIONS ON VEHICULAR TECHNOLOGY, *KSII Transactions on Internet and Information Systems*, *Transactions on Emerging Telecommunications Technologies*, and *China Communications*.

Xing Wei received the B.S. degree in electronic engineering from Beijing Institute of Technology, Beijing, China, in 2015. Her research interests include array signal processing and convex optimization.